OPEN ACCESS
IOP Publishing
Journal of Physics B: Atomic, Molecular and Optical Physics
J. Phys. B: At. Mol. Opt. Phys. **58** (2025) 075203 (19pp)
https://doi.org/10.1088/1361-6455/adbfe9

Electron–positronium scattering and Ps^- photodetachment

William Mitchell and S J Ward*

Department of Physics, University of North Texas, Denton, TX 76203, United States of America

E-mail: Sandra.Quintanilla@unt.edu and WilliamMitchell3@my.unt.edu

Received 11 November 2024, revised 7 February 2025
Accepted for publication 12 March 2025
Published 31 March 2025

Abstract

We investigate the fundamental three-body Coulomb process of elastic electron–positronium (e^--Ps) scattering below the Ps($n=2$) threshold. Using the complex Kohn variational method and trial wave functions that contain highly correlated Hylleraas-type terms, we accurately compute ^{1,3}S-, ^{1,3}P-, and ^{1,3}D-wave phase shifts, which may be considered as benchmark results. We explicitly investigate the effect of the mixed symmetry term in the short-range part of the ^{1,3}D-wave trial wave function on the phase shifts and resonances. Using the complex Kohn phase shifts we compute, for e^--Ps scattering, the elastic differential, elastic integrated, momentum-transfer, and ortho-para conversion cross sections and determine the importance of the complex Kohn D-wave phase shifts on these cross sections. In addition, using the short-range part of the ^{1}S-wave trial wave function for the bound-state of the purely leptonic ion of Ps^-, and the complex Kohn ^{1}P trial wave function for the continuum state, we determine the Ps^- photodetachment cross section in the length, velocity, and acceleration forms.

Keywords: elastic electron scattering, positronium, photodetachment

1. Introduction

In 2011, Michishio and co-workers published an experimental measurement of the photodetachment of the positronium negative ion (Ps^-) through a new technique to produce the ions efficiently using a sodium coated tungsten surface [1]. Their experimental techniques to produce an energy-tunable positronium (Ps) beam were further detailed [2], and then improved [3]. Michishio and co-workers have experimentally observed the shape resonance just above the Ps($n=2$) threshold [4], have performed threshold photodetachment spectroscopy [5], and very recently have performed anisotropic photodetachment of Ps^- ions with linearly polarized light [6]. Nagashima has presented a report on experiments on Ps^- ions [7], and more recently, Nagashima *et al* have reviewed the production of an energy-tunable Ps beam via Ps^- photodetachment [8]. An important use of Ps is to create antihydrogen in the AEgIS [9–11] and the GBAR [12] experiments at CERN very recently, Ps has been cooled to ultra-low velocities with a chirped laser pulse [13–16]. An experiment to produce the positronium positive (plus) ion (Ps^+, $e^+ + e^+ + e^-$) has been proposed by [17, 18]. The purely leptonic systems of Ps, Ps^-, and Ps^+ are ideal to be used in tests of quantum electrodynamics [19, 20]. The experimental observation of the photodetachment of Ps^- [1, 8, 21] has motivated further interest in accurate theoretical calculations.

In this paper, we present a non-relativistic treatment of e^--Ps elastic scattering below the Ps($n=2$) threshold, ignoring positron annihilation. We have presented our work at various meetings [22–31]. The excitation threshold of Ps($n=2$) occurs at $k=0.50$ a.u., where k is the magnitude of the wave vector of the electron relative to the center-of-mass of Ps, which corresponds to an incident energy E_i of approximately 5.102 eV. (We use the conversion factor of 1 a.u. = 27.211 386 245 988 eV [32]). There have been prior calculations of ^{1,3}S and ^{1,3}P e^--Ps elastic scattering below the

* Author to whom any correspondence should be addressed.

Original Content from this work may be used under the terms of the Creative Commons Attribution 4.0 licence. Any further distribution of this work must maintain attribution to the author(s) and the title of the work, journal citation and DOI.

© 2025 The Author(s). Published by IOP Publishing Ltd

Ps($n = 2$) threshold that employed the Kohn and inverse Kohn variational methods. However, we use in addition to the Kohn and inverse Kohn variational methods for ^{1,3}S- and ^{1,3}P-wave scattering, the complex Kohn variational method. Cooper *et al* [33, 34] have demonstrated that the complex Kohn variational method has less singularities than either the Kohn or inverse Kohn methods. The Kohn-type variational methods can provide benchmark results for the phase shifts of e^--Ps scattering to which results from other methods can be compared.

We apply the complex Kohn, Kohn, and inverse Kohn variational methods to ^{1,3}D-wave e^--Ps scattering to compute the phase shifts. Previously, the ^{1,3}D-wave phase shifts have been approximately obtained using the static exchange and adiabatic exchange methods, as well as the O'Malley *et al* [35] effective range theory (ERT) [36, 37]. However, to our knowledge there has been only one paper previously that has reported accurate ^{1,3}D-wave phase shifts, using the close-coupling method [38]. Furthermore, we study the effect of a mixed symmetry term that is in the short-range portion of the ^{1,3}D trial wave function. We explicitly investigate the effect of this term in the phase shifts and resonances. In the four-body Ps-H scattering problem, Woods *et al* [39] ignored the mixed symmetry term in their calculation due to the difficulty of including it. Wu *et al* [40, 41] have since attributed the differences in their results of the same system to this missing term in the calculation of Woods *et al* [39]. We also compute the elastic differential, elastic integrated, momentum-transfer, and ortho-para conversion cross sections and study the effect of including accurate D-wave phase shifts in these calculations. Importantly, the e^--Ps results can be used as mass-scaled benchmarks for proton-protonium calculations that are of interest in antihydrogen-H_2 interactions [42, 43].

We use a highly-correlated Hylleraas-type ^{1}S trial wave function, that includes all interparticle distances, to determine the binding energy of Ps^-. Using this bound-state wave function of Ps^-, its binding energy, and the complex Kohn ^{1}P continuum wave function we accurately calculate the Ps^- photodetachment cross section in the length, velocity, and acceleration forms. There have been prior accurate calculations of the Ps^- photodetachment cross section in the length and velocity forms [38, 44], but to our knowledge this is the first paper reporting the cross section in the acceleration form. Importantly, we resolve the long-standing discrepancy between the calculation of the Ps^- photodetachment cross section of Ward *et al* [37] who used for the ^{1}P continuum the Kohn trial wave function with the calculations of Igarashi *et al* [38] and Igarashi *et al* [44] who used close-coupling wave functions.

There have been a number of prior calculations of phase shifts and cross sections for e^--Ps scattering, resonance calculations of the e^--Ps system, and calculations of the binding energy of Ps^- and the photodetachment cross section of Ps^-. The present calculations are an extension of the prior calculations of the Kohn and inverse Kohn ^{1,3}S- and ^{1,3}P-wave phase shifts, ^{1}S and ^{1,3}P resonance parameters, binding energy, photodetachment, and scattering cross section calculations given in [36, 37, 45–49]. Basu and Ghosh [50, 51] performed 3- and 6-state close-coupling calculations to determine the ^{1,3}S- and ^{1,3}P-wave phase shifts for e^--Ps scattering, while Igarashi *et al* performed 18- and 27-state close-coupling calculations with B-splines to determine the ^{1,3}S-, ^{1,3}P-, ^{1,3}D-, and ^{1,3}F-wave phase shifts [38].

Binding energy calculations have been previously performed by Bhatia and Drachman using a Hylleraas wave function [52], by Ho using a 946-term Hylleraas-type wave function [53] and a double-basis set Hylleraas-type function [54], by Kar and Ho [55], by Frolov [56–58], and by Korobov [59] using exponential functions, and by Drake *et al*. using a triple basis set in Hylleraas coordinates with 2528 terms [60]. It has also been determined by Haftel and Mandelzweig using the correlation function hyperspherical method [61], by Gilmore *et al* using a 9-state coupled pseudostate approximation [62], by Blinov and Czarnecki using dimensional scaling [63], and by Duan *et al* [64] using generalized harmonic polynomials.

A pioneering photodetachment cross section calculation of Ps^- has been performed by Bhatia and Drachman [65, 66]. They used an asymptotic form of the bound-state wave function and a plane-wave treatment for the final-state wave function. Later, Frolov applied the long-range, asymptotic approximation using the asymptotic form of the bound-state wave function that he obtained from his accurate Ps^- wave function [58]. The photodetachment cross section has also been calculated by Ermolaev and Mandal using a one-active-electron model with a two-center atomic orbital expansion [67], by Ghoshal and Ho using exponential cosine-screened Coulomb potentials [68], and by Igarashi *et al* using the hyperspherical close-coupling method [44], and Igarashi *et al* using the close-coupling method with a B-spline expansion [38]. Bhatia has recently computed cross sections for Ps^- photodetachment into various excited P states of Ps in which he used the asymptotic form of a Ps^- bound-state wave function [65] and a plane wave for the final state [69]. Maniadaki *et al* have calculated the photodetachment cross section using a configuration interaction method on a B-splines basis [70]. The Ps^- photodetachment cross section has recently been computed using the complex coordinate rotation method with Gaussian basis functions [71]. All of these previous calculations have reported the cross section in both the length and velocity forms, or only the length form.

Resonance positions and widths for the e^--Ps system have been reported by Ho [72] and by Bhatia and Ho [73, 74] who used the complex coordinate rotation method with Hylleraas-type functions. They have also been given by Kar and Ho [55, 75–78] and Kar *et al* [79] who used exponential functions. Furthermore, they have also been determined by Basu and Ghosh [50, 51, 80, 81] using 3-, 6-, and 9-state close-coupling approximations, by Gilmore *et al* using a 9-state coupled pseudostate approximation [62], by Usukura and Suzuki using the stochastic variational method combined with the complex scaling method [82], by Igarashi *et al* who did a time-delay matrix analysis of their hyperspherical close-coupling results [83], and by Igarashi using the complex rotation method with hyperspherical coordinates [84]. In addition, Botero [85] and Botero and Greene [86, 87] have obtained resonances using

the adiabatic method with hyperspherical coordinates while Zhou and Lin employed the hyperspherical close-coupling method and obtained $^1S^e$ resonances below the Ps($n=2$) and Ps($n=3$) thresholds [88].

The ^{1,3}S scattering length calculations have been performed by Bhatia and Drachman using their bound-state Ps^- function [66] and Kvitsinsky *et al* using the Faddeev equations [89]. Ghoshal *et al* have determined the ^{1}S scattering length using their variational Ps^- wave function and an ERT [90]. Various cross sections for e^--Ps scattering have been calculated by Igarashi *et al* [91] using the hyperspherical close-coupling method, Basu and Ghosh using a 6-state close-coupling approximation [50, 51], Gilmore *et al* using 9- and 30-state coupled pseudostate approximations [62], Kvitsinsky *et al* using the Faddeev equations [89], and Melezhik and Vukajlović using the adiabatic method [92].

Section 2 of this paper presents the application of the complex Kohn, Kohn, and inverse Kohn variational methods to e^--Ps scattering below the Ps($n=2$) threshold. It also presents the trial wave functions that we use in the scattering and bound-state calculations, a resonance fitting formula, a few ERT formulas, and information on the Ps^- binding energy calculation. Furthermore, it gives expressions for the Ps^- photodetachment cross section in length, velocity, and acceleration forms, and finishes with formulas for scattering cross sections. Section 3 presents the ^{1,3}S- and ^{1,3}P-wave phase shifts for e^--Ps scattering, ^{1}S-, ^{1,3}P-, and ^{1,3}D-wave resonance parameters, ^{1,3}S-wave scattering lengths, and the Ps^- binding energy. It also gives the Ps^- photodetachment cross section in the length, velocity, and acceleration forms. Furthermore, it gives the ^{1,3}D-wave phase shifts, and specifically, the effect of the mixed symmetry term in the ^{1,3}D-wave trial wave function on the phase shifts and resonances. Finally, it gives various scattering cross sections. Section 4 presents our concluding remarks. Appendix A provides further numerical details for the calculations of the binding energy, phase shifts, scattering lengths, and resonance parameters, as well as giving the Kohn and inverse Kohn phase shifts for the ^{1,3}S- and ^{1,3}P-waves. Appendix B gives numerical details for the photodetachment calculation. Note that we use atomic units throughout unless stated otherwise.

2. Theory

2.1. Elastic e^--Ps scattering and Kohn-type variational methods

Figure 1 shows the coordinate diagram for the e^--Ps system where $(\boldsymbol{r}_1, \boldsymbol{r}_2)$ are the position vectors of the two electrons with respect to the position of the positron, and $r_3 = |\boldsymbol{r}_2 - \boldsymbol{r}_1|$ is the inter-electronic distance [36, 37]. The Jacobi coordinates for when electron 2 is bound and electron 1 is incident are $(\boldsymbol{r}_2, \boldsymbol{\rho} = \boldsymbol{r}_1 - \frac{1}{2}\boldsymbol{r}_2)$, while the corresponding exchange Jacobi coordinates for when electron 1 is bound and electron 2 is incident are $(\boldsymbol{r}_1, \boldsymbol{\rho}' = \boldsymbol{r}_2 - \frac{1}{2}\boldsymbol{r}_1)$. In the center of mass frame, the Hamiltonian for the system can be expressed as,

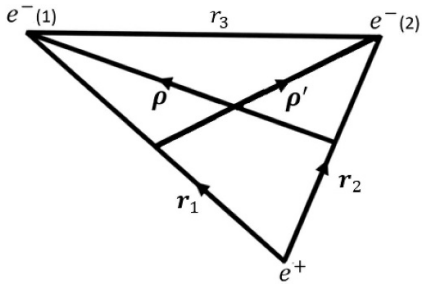

Figure 1. The e^--Ps coordinate system.

$$H = -\frac{1}{2\mu_1}\nabla^2_{\boldsymbol{r}_2} - \frac{1}{2\mu_2}\nabla^2_{\boldsymbol{\rho}} - \frac{1}{r_1} - \frac{1}{r_2} + \frac{1}{r_3}, \tag{1}$$

where

$$\mu_1 = \mu(\mathrm{Ps}) = \frac{1}{2} \quad \text{and} \quad \mu_2 = \mu\left(\mathrm{Ps}^-\right) = \frac{2}{3}. \tag{2}$$

The derivation and notation of the Kohn-type variational methods that we present here largely follows that of [39]. The functional for the scattering trial wave function $\Psi_l^{\pm,t}$ is given by,

$$I\left[\Psi_l^{\pm,t}\right] = \left(\Psi_l^{\pm,t}\mathcal{L}\Psi_l^{\pm,t}\right), \tag{3}$$

where l represents the partial wave, t indicates trial, the plus and minus signs indicate the singlet and triplet, respectively, and

$$\mathcal{L} = 2\mu_2(H - E), \tag{4}$$

in which the total energy of the system is given by,

$$E = E_{\mathrm{Ps}} + \frac{k^2}{2\mu_2}, \tag{5}$$

where $E_{\mathrm{Ps}} = -1/4$ is the ground-state energy of Ps. We are assuming the trial wave function is a small variation $\delta\Psi_l^{\pm}$ from the exact wave function $\Psi_l^{\pm}$,

$$\Psi_l^{\pm,t} = \Psi_l^{\pm} + \delta\Psi_l^{\pm}. \tag{6}$$

The variational in the functional is given by,

$$\delta[I] = \left(L^{\pm,t} - L^{\pm}\right)\det\boldsymbol{u} + I\left[\delta\Psi_l^{\pm}\right], \tag{7}$$

where $L^{\pm,t}$ represents the scattering quantity in the trial wave function and $L^{\pm}$ is the corresponding quantity for the exact wave function. Realizing that $I[\Psi_l^{\pm}] = 0$ and neglecting $I[\delta\Psi_l^{\pm}]$, which is a second order term in $\delta\Psi_l^{\pm}$, yields the functional for the variational (v) quantity $L^{\pm,v}$,

$$L^{\pm,v} = L^{\pm,t} - I\left[\Psi_l^{\pm}\right]/\det\boldsymbol{u}. \tag{8}$$

For the complex Kohn variational method we have,

$$L_l^{\pm,t} = -S_l^{\pm,t} = -\mathrm{e}^{2\mathrm{i}\delta_l^{\pm,t}}, \quad \boldsymbol{u} = \begin{bmatrix} -i & 1 \\ i & 1 \end{bmatrix}, \tag{9}$$

for the Kohn,

$$L_l^{\pm,t} = K_l^{\pm,t} = \tan\delta_l^{\pm,t}, \quad \boldsymbol{u} = \begin{bmatrix} 1 & 0 \\ 0 & 1 \end{bmatrix}, \tag{10}$$

and for the inverse Kohn,

$$L_l^{\pm,t} = -\left(K_l^{\pm,t}\right)^{-1} = -\cot\delta_l^{\pm,t}, \quad \boldsymbol{u} = \begin{bmatrix} 0 & 1 \\ -1 & 0 \end{bmatrix}. \tag{11}$$

The complex Kohn method gives less singularities than the Kohn or inverse Kohn methods [33, 34].

Using the stationary property of the functional, one sets the derivatives of the functional $L^{\pm,v}$, equation (8), with respect to each linear parameter to zero. For the S-wave, one has

$$\frac{\partial L^{\pm,v}}{\partial L^{\pm,t}} = 0 \quad \text{and} \quad \frac{\partial L^{\pm,v}}{\partial a_j^{\pm}} = 0, \; j = 1,\ldots,N, \tag{12}$$

where $a_j^{\pm}$ represents the linear parameters in the short-range part of the trial scattering wave function and N is the number of terms in this part. Equation (12) leads to a set of $(N+1)$ linear equations which can be written in a matrix equation [39, 93–95], $AX = -B$,

$$\begin{bmatrix} \left(\tilde{C}\mathcal{L}\tilde{C}\right) & \left(\tilde{C}\mathcal{L}\varphi_1^{\pm}\right) & \ldots & \left(\tilde{C}\mathcal{L}\varphi_N^{\pm}\right) \\ \left(\varphi_1^{\pm}\mathcal{L}\tilde{C}\right) & \left(\varphi_1^{\pm}\mathcal{L}\varphi_1^{\pm}\right) & \ldots & \left(\varphi_1^{\pm}\mathcal{L}\varphi_N^{\pm}\right) \\ \vdots & \vdots & \ddots & \vdots \\ \left(\varphi_N^{\pm}\mathcal{L}\tilde{C}\right) & \left(\varphi_N^{\pm}\mathcal{L}\varphi_1^{\pm}\right) & \ldots & \left(\varphi_N^{\pm}\mathcal{L}\varphi_N^{\pm}\right) \end{bmatrix} \begin{bmatrix} L^{\pm,t} \\ a_1^{\pm} \\ \vdots \\ a_N^{\pm} \end{bmatrix} = -\begin{bmatrix} \left(\tilde{C}\mathcal{L}\tilde{S}\right) \\ \left(\varphi_1^{\pm}\mathcal{L}\tilde{S}\right) \\ \vdots \\ \left(\varphi_N^{\pm}\mathcal{L}\tilde{S}\right) \end{bmatrix}. \tag{13}$$

We give the definitions of $\tilde{C}, \tilde{S}$ and $\varphi_j^{\pm}$ in section 2.2. Finally, we solve for $L^{\pm,v}$,

$$L^{\pm,v} = -\frac{1}{\det \boldsymbol{u}}\left[B^T X + \left(\tilde{S}\mathcal{L}\tilde{S}\right)\right], \tag{14}$$

to obtain the phase shifts.

2.2. Trial wave functions

In this section we present trial wave functions for ^{1,3}S-, ^{1,3}P-, and ^{1,3}D-wave e^--Ps scattering that we use for all three Kohn-type variational methods. We give the results of these calculations in section 3 and appendix A.

A general from for the trial wave function of partial wave l for e^--Ps elastic scattering is given by,

$$\Psi_l^{t,\pm} = \sqrt{\frac{k}{2}}\left(1 \pm P_{12}\right)\varphi_{\mathrm{Ps}}\left(r_2\right) Y_{l0}\left(\theta_\rho, \varphi_\rho\right)\left(\tilde{S}_l + L_l^{\pm,t}\tilde{C}_l\right) + \sum_{i=1}^{l+1}\Phi_i^{\pm}, \tag{15}$$

where P_{12} is a permutation operator that interchanges the spatial coordinates of the two electrons, and $\varphi_{\mathrm{Ps}}(r_2)$ is the exact wave function of Ps(1s) which is given by,

$$\varphi_{\mathrm{Ps}}\left(r_2\right) = \frac{1}{\sqrt{8\pi}} e^{-r_2/2}, \tag{16}$$

and where θ_ρ and φ_ρ are the polar and the azimuthal angles, respectively, of $\boldsymbol{\rho}$. The trial wave function has a long-range part, $\sqrt{k/2}(1 \pm P_{12})\varphi_{\mathrm{Ps}}(r_2)Y_{l0}(\theta_\rho,\varphi_\rho)(\tilde{S}_l + L_l^{\pm,t}\tilde{C}_l)$, and a short-range part, $\sum\Phi_i^{\pm}$, that is a highly correlated function which includes all interparticle distances. The long-range terms $(\tilde{S}_l, \tilde{C}_l)$ are given by

$$\begin{bmatrix} \tilde{S}_l \\ \tilde{C}_l \end{bmatrix} = \boldsymbol{u}\begin{bmatrix} \bar{S}_l \\ \bar{C}_l \end{bmatrix} = \begin{bmatrix} u_{00} & u_{01} \\ u_{10} & u_{11} \end{bmatrix}\begin{bmatrix} \bar{S}_l \\ \bar{C}_l \end{bmatrix}, \tag{17}$$

where

$$\bar{S}_l = j_l(k\rho), \quad \text{and} \quad \bar{C}_l = -n_l(k\rho)\left(1 - e^{-\mu\rho}\right)^n, \tag{18}$$

in which $j_l(k\rho)$ and $n_l(k\rho)$ are the spherical Bessel and Neumann functions, respectively. Present in the $\bar{C}_l$ definition is a shielding function that removes the singularity of the spherical Neumann function which is at the origin. The value for the power of the shielding function n, and the nonlinear variational parameter μ, varies for each partial wave. We give the values of n and μ that we use in appendix A. Due to azimuthal symmetry the magnetic quantum number m is zero in the spherical harmonic $Y_{lm}(\theta_\rho, \varphi_\rho)$ in the long-range part of the trial wave function.

For the short-range part, there are $l+1$ different symmetries [96]. For the ^{1,3}S-wave, the short-range part of the trial wave function is a Hylleraas-type function given by,

$$\Phi_0^{\pm} = \frac{1}{\sqrt{2}} Y_{00}\left(\theta_\rho, \varphi_\rho\right)\sum_{j=1}^{N} a_j^{\pm}\bar{\varphi}_j^{\pm} = \sum_{j=1}^{N} a_j^{\pm}\varphi_j^{\pm}. \tag{19}$$

The short-range terms are given by,

$$\bar{\varphi}_j^{\pm} = e^{-\alpha^{\pm}s - \gamma^{\pm}r_3} s^{k_j} t^{l_j} r_3^{m_j}, \tag{20}$$

where $\alpha^{\pm}$ and $\gamma^{\pm}$ are nonlinear variational parameters and s, t, r_3 are the Hylleraas (elliptic) coordinates where $s = r_1 + r_2$ and $t = |r_1 - r_2|$. The number of terms N is determined by ω [37, 95] where,

$$l_j + k_j + m_j \leqslant \omega, \tag{21}$$

and l_j,k_j,m_j, and ω are non-negative integers. For the S-wave l_j must be even for the singlet case, and odd for the triplet case. We give in table 1 the number of terms N for a given ω for the ^{1,3}S, ^{1,3}P, and ^{1,3}D trial scattering wave functions.

For the ^{1,3}P-wave, the short-range part of the trial wave function is given by,

Table 1. Number of total short-range terms N for each e^--Ps scattering trial wave function for a given ω, where ω is given by equation (21).

ω	N ^{1}S (^{3}S)	N ^{1,3}P	N ^{1}D (^{3}D)
1	3 (1)	4	7 (5)
2	7 (3)	10	17 (13)
3	13 (7)	20	33 (27)
4	22 (13)	35	57 (48)
5	34 (22)	56	90 (78)
6	50 (34)	84	134 (118)
7	70 (50)	120	190 (170)
8	95 (70)	165	260 (235)
9	125 (95)	220	345 (315)
10	161 (125)	286	447 (411)
11	203 (161)	364	567 (525)
12	252 (203)	455	707 (658)
13	308 (252)	560	868 (812)
14	372 (308)	680	1052 (988)
15	444 (372)	816	1260 (1188)

$$\sum_{i=1}^{2}\Phi_i^{\pm} = \frac{1}{\sqrt{2}}\left(Y_{10}(\theta_\rho,\varphi_\rho)\,\rho \pm Y_{10}(\theta_{\rho'},\varphi_{\rho'})\,\rho'\right)\sum_{j=1}^{N_1} a_j^{\pm}\bar{\varphi}_j^{\pm} + \frac{1}{\sqrt{2}}\left(Y_{10}(\theta_\rho,\varphi_\rho)\,\rho \mp Y_{10}(\theta_{\rho'},\varphi_{\rho'})\,\rho'\right)\sum_{j=N_1+1}^{N} b_j^{\pm}\bar{\varphi}_j^{\pm}, \tag{22}$$

where $\theta_{\rho'}$ and $\varphi_{\rho'}$ are the polar and the azimuthal angles, respectively, of $\boldsymbol{\rho}'$, and where l_j is even in the first summation and odd in the second summation. Furthermore, N_1 is the number of short-range terms where l_j is even, and N is the total number of short-range terms. The linear variational parameters are $a_j^{\pm}$ and $b_j^{\pm}$.

For the ^{1,3}D-wave, the short-range part of the trial wave function is given by,

$$\begin{aligned}\sum_{i=1}^{3}\Phi_i^{\pm} = {}& \frac{1}{\sqrt{2}}\left(Y_{20}(\theta_\rho,\varphi_\rho)\,\rho^2 \pm Y_{20}(\theta_{\rho'},\varphi_{\rho'})\,\rho'^2\right)\sum_{j=1}^{N_1} a_j^{\pm}\bar{\varphi}_j^{\pm} \\ & + \frac{1}{\sqrt{2}}\left(Y_{20}(\theta_\rho,\varphi_\rho)\,\rho^2 \mp Y_{20}(\theta_{\rho'},\varphi_{\rho'})\,\rho'^2\right)\sum_{j=N_1+1}^{N_2} b_j^{\pm}\bar{\varphi}_j^{\pm} \\ & + \frac{1}{\sqrt{2}}\rho\rho'\left(Y_{11}(\theta_\rho,\varphi_\rho)\,Y_{1,-1}(\theta_{\rho'},\varphi_{\rho'})\right. \\ & + Y_{10}(\theta_\rho,\varphi_\rho)\,Y_{10}(\theta_{\rho'},\varphi_{\rho'}) \\ & \left. + Y_{1,-1}(\theta_\rho,\varphi_\rho)\,Y_{11}(\theta_{\rho'},\varphi_{\rho'})\right)\sum_{j=N_2+1}^{N} c_j^{\pm}\bar{\varphi}_j^{\pm},\end{aligned} \tag{23}$$

where l_j is even in the first summation, odd in the second summation, and even (odd) in the third summation for the singlet (triplet) case. Again N_1 is the number of short-range terms in the first symmetry, N_2 is the number of short-range terms in the first two symmetries, and N is the total number of short-range terms. The linear variational parameters are $a_j^{\pm}, b_j^{\pm}$, and $c_j^{\pm}$. The third summation of the ^{1,3}D-wave short-range part of the trial wave function (RHS of equation (23)) is referred to as the mixed symmetry term. In section 3.5 we discuss its importance to the ^{1,3}D-wave phase shifts and its effect on the resonances. In section 3.6 we discuss the significance of the complex Kohn D-wave phase shifts in the scattering cross sections.

2.3. Resonances

Below the Ps($n=2$) threshold there are Feshbach resonances [97] in the e^--Ps system. In section 3 we compare the resonance parameters that we obtain with those found in the literature [36, 37, 62, 72–75, 82, 83, 86]. We compute the positions and widths for the Feshbach resonances using the Breit-Wigner formula [98–100] with a slowly varying background of the form [101, 102],

$$\delta(E) = \tan^{-1}\frac{\Gamma_{\rm res}}{2(E-E_{\rm res})} + \sum_{i=0}^{2}(E)^i, \tag{24}$$

where

$$\delta^{\rm res} = \tan^{-1}\frac{\Gamma_{\rm res}}{2(E-E_{\rm res})}, \tag{25}$$

$E_{\rm res}$ is the position of the resonance, and $\Gamma_{\rm res}$ is the full width at half maximum.

2.4. Effective range theories

In order to calculate the ^{1,3}S-wave scattering lengths $a_0^{\pm}$ we employ ERT formulas that were derived by explicitly taking into account the polarization potential for e^--Ps elastic scattering. The first is the ERT formula provided by O'Malley *et al* [35] given by,

$$k\cot\delta_0^{\pm} = -\frac{1}{a_0^{\pm}} + \frac{\pi\mu_2\alpha}{3\left(a_0^{\pm}\right)^2}k + \frac{2\mu_2\alpha}{3a_0^{\pm}}k^2\ln\left(\frac{\mu_2\alpha}{16}k^2\right), \tag{26}$$

where $\alpha = 36$ is the electric dipole polarizability of Ps(1s).

The second is the ERT formula provided by Bransden [103],

$$\tan\delta_0^{\pm} = -a_0^{\pm}k - \frac{\pi\mu_2\alpha}{3}k^2 - \frac{4\mu_2\alpha}{3}a_0^{\pm}k^3\ln(k), \tag{27}$$

which is derived from equation (4.3) of O'Malley *et al* [35]. (The procedure to obtain equation (27) is given by Macek [104]. Levy and Keller obtained the expression for the phase shift δ_0 rather than for $\tan\delta_0$ [105]). We use Mathematica [106] to fit both of these ERT formulas to the Kohn-type variational ^{1,3}S phase shifts in order to determine the scattering lengths and to obtain the R^2 values for the fits.

In the elastic integrated, momentum-transfer, and ortho-para conversion cross sections we use the ^{1,3}F-wave phase shifts that we determine using the O'Malley *et al* [35] ERT formula for $l \geqslant 1$, which is given by,

$$\tan\delta_l = \frac{\mu_2\alpha\pi k^2}{(2l-1)(2l+1)(2l+3)}. \tag{28}$$

We give the results of the scattering cross sections in section 3.6.

2.5. Binding energy of Ps^-

For the calculation of the binding energy E_b of Ps^- it is more convenient to use the center of mass Hamiltonian expressed solely in terms of $\boldsymbol{r}_1$ and $\boldsymbol{r}_2$, which is given by,

$$H = -\frac{1}{2\mu_1}\nabla^2_{\boldsymbol{r}_1} - \frac{1}{2\mu_1}\nabla^2_{\boldsymbol{r}_2} - \nabla_{\boldsymbol{r}_1}\cdot\nabla_{\boldsymbol{r}_2} - \frac{1}{r_1} - \frac{1}{r_2} + \frac{1}{r_3}, \quad (29)$$

where $-\nabla_{\boldsymbol{r}_1}\cdot\nabla_{\boldsymbol{r}_2}$ is the mass polarization term [107].

We use for the bound-state wave function of Ps^- the short-range part of the ^{1}S-wave trial wave function, equation (19), and the Rayleigh–Ritz variational method, to determine the binding energy of Ps^-. Not only does this calculation provide confidence in the accuracy of the short-range terms to describe the Ps^- system, but an accurate binding energy is important for a reliable determination of the Ps^- photodetachment cross section. Note that we optimize the values of both of the non-linear variational parameters of equation (20), α^+ and γ^+, for this binding energy calculation separate from the phase shift calculations. We give our choice of nonlinear parameters in table A1 in appendix A.

2.6. The photodetachment of Ps^-

Time-dependent perturbation theory is used to derive the expressions for the photodetachment cross section for Ps^- [36, 37, 47]. The length (L) form of the cross section is given by,

$$\sigma_\lambda(L) = 6.8115\times10^{-20}k\left(k^2+\gamma^2\right)|\mu^L|^2 \ \text{cm}^2, \quad (30)$$

where,

$$\gamma^2 = 2\mu_2 E_b, \quad (31)$$

and the length matrix element is,

$$\mu^L = \hat{\boldsymbol{k}}\cdot\langle\Psi_f|\boldsymbol{r}_2 + \mu_2\boldsymbol{\rho}|\Psi_i\rangle, \quad (32)$$

in which $\hat{\boldsymbol{k}}$ is the direction of the wave vector of the ejected electron with respect to the center-of-mass of Ps. The velocity (V) form of the cross section is given by,

$$\sigma_\lambda(V) = 2.7246\times10^{-19}\mu_2^2\frac{k}{k^2+\gamma^2}|\mu^V|^2 \ \text{cm}^2, \quad (33)$$

where the velocity matrix element is,

$$\mu^V = \hat{\boldsymbol{k}}\cdot\langle\Psi_f|\frac{1}{\mu_1}\nabla_{\boldsymbol{r}_2} + \nabla_{\boldsymbol{\rho}}|\Psi_i\rangle. \quad (34)$$

The acceleration (A) form of the cross section is given by,

$$\sigma_\lambda(A) = 1.2109\times10^{-19}\mu_2^2\frac{16k}{\left(k^2+\gamma^2\right)^3}|\mu^A|^2, \quad (35)$$

where the acceleration matrix element is,

$$\mu^A = \hat{\boldsymbol{k}}\cdot\langle\Psi_f|\frac{\boldsymbol{r}_1}{r_1^3} + \frac{\boldsymbol{r}_2}{r_2^3}|\Psi_i\rangle. \quad (36)$$

Choosing the z-axis to be parallel to $\hat{\boldsymbol{k}}$ gives,

$$\mu^L_z = \langle\Psi_f|z_2 + \mu_2\rho_z|\Psi_i\rangle, \quad (37)$$

$$\mu^V_z = \langle\Psi_f|\frac{1}{\mu_1}\frac{\partial}{\partial z_2} + \frac{\partial}{\partial\rho_z}|\Psi_i\rangle, \quad (38)$$

$$\mu^A = \langle\Psi_f|\frac{z_1}{r_1^2} + \frac{z_2}{r_2^2}|\Psi_i\rangle. \quad (39)$$

We compute the Ps^- photodetachment cross section in the length, velocity, and acceleration forms for energies below the Ps($n=2$) threshold. In the matrix elements of equations (32), (34) and (36), Ψ_i is the wave function for the ^{1}S bound-state of Ps^- given by equations (19) and (20) and Ψ_f is the ^{1}P continuum wave function of the e^--Ps system, which is normalized according to,

$$\langle\Psi_{f'}|\Psi_f\rangle = (2\pi)^3\delta(\boldsymbol{k'}-\boldsymbol{k}). \quad (40)$$

For the ^{1}P continuum wave function, to obtain the normalization of equation (40) one needs to multiply the complex Kohn ^{1}P trial wave function given by equations (9), (15), (17), (18) and (22) by the factor $\mathrm{i}/2\sqrt{12\pi/k}\mathrm{e}^{-\mathrm{i}\delta_1^+}$, where δ_1^+ is the complex Kohn ^{1}P trial phase shift. However, for the Kohn ^{1}P trial wave function given by equations (10), (15), (17), (18) and (22), one needs to multiply it by the factor $\sqrt{12\pi/k}\cos\delta_1^+$. Although we compute the photodetachment cross section using both the complex Kohn and Kohn ^{1}P trial wave functions, we present results in this paper using only the complex Kohn. We note that Ward *et al* [37] multiplied their Kohn ^{1}P trial wave function by $\sqrt{12\pi/k}$, but they did not multiply it by $\cos\delta_1^+$. This means that their normalization of Ψ_f did not satisfy equation (40). However, multiplying their photodetachment cross section (in length and velocity forms) by the factor $\cos^2\delta_1^+$ brings their results in accord with the cross section computed by Igarashi *et al* [38] and by Igarashi *et al* [44]. Importantly, this resolves the discrepancy between these different sets of prior results.

2.7. Scattering cross sections

We calculate various cross sections for e^--Ps scattering and we study the importance of the D-wave complex Kohn phase shifts on these cross sections. We compute the elastic integrated cross section σ_{el}, the elastic differential cross section $\mathrm{d}\sigma_{\mathrm{el}}/\mathrm{d}\Omega$, the momentum-transfer cross section σ_{m} [103], and the ortho-para conversion cross section σ_{c}. The formulas for these cross sections are given by,

$$\sigma^\pm_{\mathrm{el}}\left(k^2\right) = \frac{4}{k^2}\sum_{l=0}^{\infty}(2l+1)\sin^2\delta_l^\pm \quad \left[\pi a_0^2\right], \quad (41)$$

$$\frac{\mathrm{d}\sigma^\pm_{\mathrm{el}}}{\mathrm{d}\Omega}(\theta,k) = \left|\sum_{l=0}^{\infty}\frac{1}{2ik}(2l+1)\left(\mathrm{e}^{2\mathrm{i}\delta_l^\pm}-1\right)P_l(\cos\theta)\right|^2 \quad \left[a_0^2 sr^{-1}\right], \quad (42)$$

$$\sigma_{\rm m}^{\pm}\left(k^2\right)=\frac{4}{k^2}\sum_{l=0}^{\infty}(l+1)\sin^2\left(\delta_l^{\pm}-\delta_{l+1}^{\pm}\right)\quad\left[\pi a_0^2\right], \tag{43}$$

$$\sigma_{\rm c}\left(k^2\right)=\frac{1}{4k^2}\sum_{l=0}^{\infty}(2l+1)\sin^2\left(\delta_l^{+}-\delta_l^{-}\right)\quad\left[\pi a_0^2\right]. \tag{44}$$

Baltenko and Segal [108] discusses ortho-para conversion of Ps in a cool plasma.

In an unpolarized beam of electrons there will be three times as many electrons in the triplet state as the singlet state, and thus the spin-weighted cross section formulas are given by,

$$\sigma_{\rm el}=\frac{1}{4}\left(\sigma_{\rm el}^{+}+3\sigma_{\rm el}^{-}\right)\quad\left[\pi a_0^2\right], \tag{45}$$

$$\frac{{\rm d}\sigma_{\rm el}}{{\rm d}\Omega}=\frac{1}{4}\left(\frac{{\rm d}\sigma_{\rm el}^{+}}{{\rm d}\Omega}+3\frac{{\rm d}\sigma_{\rm el}^{-}}{{\rm d}\Omega}\right)\quad\left[a_0^2 sr^{-1}\right], \tag{46}$$

$$\sigma_{\rm m}=\frac{1}{4}\left(\sigma_{\rm m}^{+}+3\sigma_{\rm m}^{-}\right)\quad\left[\pi a_0^2\right]. \tag{47}$$

We give in section 3.6 the zero-energy limits of the cross sections that we calculate using the singlet a_0^+ and triplet a_0^- S-wave scattering lengths. The formulas for the zero-energy cross sections are,

$$\sigma_{\rm el}(0)=\sigma_{\rm m}(0)=\left(a_0^{+}\right)^2+3\left(a_0^{-}\right)^2\quad\left[\pi a_0^2\right], \tag{48}$$

$$\frac{{\rm d}\sigma_{\rm el}}{{\rm d}\Omega}(\theta,0)=\frac{1}{4}\left[\left(a_0^{+}\right)^2+3\left(a_0^{-}\right)^2\right]\quad\left[a_0^2 sr^{-1}\right], \tag{49}$$

$$\sigma_{\rm c}(0)=\frac{1}{4}\left(a_0^{+}-a_0^{-}\right)^2\quad\left[\pi a_0^2\right]. \tag{50}$$

3. Results

3.1. ^{1,3}S-wave phase shifts and resonances

We compute the ^{1,3}S-wave phase shifts using the complex Kohn, Kohn, and inverse Kohn variational methods. Although the Kohn-type variational methods do not provide a rigorous upper bound on the results, one finds that in general there is an empirical upper bound. Generally, the higher the ω value, the larger the phase shift results will be due to the additional terms present in the short-range part of the trial wave functions. However, in these calculations linear dependence can cause anomalous behavior in the phase shift results when computed with an ω value that is too large. Therefore, a balance must be achieved in selecting an ω large enough to produce a numerically converged result while avoiding linear dependence. We discuss in appendix A the numerical work for the phase shift calculations.

In tables 2 and 3 we present the ^{1}S-wave and ^{3}S-wave phase shifts, respectively, that we compute with the complex Kohn variational method. We compare these results with the previous calculations that used the Kohn variational method [36], and the close-coupling calculations of Igarashi *et al* [38]. The second column of these tables show the complex Kohn phase shifts for a ω value, which we refer to as best ω, in which the convergence ratio $R(\omega)$,

$$R(\omega)=\frac{\tan\delta(\omega)-\tan\delta(\omega-1)}{0.5\left(\tan\delta(\omega)+\tan\delta(\omega-1)\right)}, \tag{51}$$

is the smallest for when the tangent of the phase shift is an increase from the previous value. There are sometimes instances where the convergence ratio is very small but the tangent of the phase shift decreases slightly. In these instances we select the smaller ω value for the best ω. The third column shows results that we generate using the lowest of these best ω values for the entire k-range. Over a majority of the k-range we consider for the singlet, and the entirety of the k-range for the triplet phase shifts, the complex Kohn best ω results are an improvement over prior Kohn-type variational results as the phase shifts are larger, and thus theoretically closer to the empirical upper bound. There are instances in table 2 where our ^{1}S complex Kohn results are slightly less than our Kohn results and those previously reported. The difference in these results is in the third significant figure and can be attributed to the choice of nonlinear parameters. The complex Kohn results agree well with those of Igarashi *et al* [38].

In table A2 of appendix A we give our Kohn and inverse Kohn ^{1,3}S phase shifts. We obtain our results using a higher, or equal, ω value for the Kohn and inverse Kohn methods compared to prior results. Our optimized Kohn results agree to at least the second decimal place with the previously reported Kohn phase shifts in tables 2 and 3 [36]. The difference between our Kohn and inverse Kohn phase shifts is at least in the third decimal place.

Table 4 presents the position and width for the ^{1}S resonance of the e$^-$-Ps system we obtain using the inverse Kohn method, along with comparisons from the literature. We compute the position and width for this resonance using the Breit-Wigner formula with a slowly varying background given by equation (24). We compute these parameters over a range of ω values from 6–12, and quote them in table 4 for $\omega=11$. These parameters for $\omega=11$ compare favorably with those in the literature. For each set of resonance parameters, we present the largest ω value that produces stable positions and widths. We find no resonances for the ^{3}S-wave.

We calculate S-wave singlet a_0^+ and triplet a_0^- scattering lengths using two different ERT formulas, equations (26) and (27), and ^{1,3}S phase shifts from the k-range of 0.000 01 to 0.001 that we obtain using the three Kohn-type variational methods. In table 5 we present the results of the calculations using the Kohn ^{1}S phase shifts and compare these results with those in the literature. Based on the R^2 value we generate by using the Mathematica fits [106], we use equation (26) for the singlet case and equation (27) for the triplet case. The scattering lengths that we use in the zero-energy cross sections are $a_0^+=11.9$ and $a_0^-=4.81$. In appendix A we give plots of the tangent of the S-wave phase shift vs. k, with our generated fits.

3.2. Binding energy

We use the Rayleigh–Ritz variational method and the ^{1}S bound-state trial wave function, equation (19), to determine

Table 2. Comparison of the complex Kohn ^{1}S-wave phase shifts δ_0^+ for e$^-$-Ps scattering with the prior Kohn [36] and 18-state close-coupling [38] results. Phase shifts are given in radians and ω is given by equation (21). For details on how we select a best ω see section 3.1 and appendix A.

k	Complex Kohn variational δ_0^+ (best ω) [present]	Complex Kohn variational δ_0^+ ($\omega = 8$) [present]	Kohn variational δ_0^+ ($\omega = 9$) [36]	Close-coupling δ_0^+ (18-state) [38]
0.05	2.554 (10)	2.554	2.544	—
0.10	2.062 (8)	2.062	2.047	2.056
0.15	1.669 (9)	1.669	1.665	—
0.20	1.391 (12)	1.345	1.376	1.378
0.25	1.155 (12)	1.155	1.154	—
0.30	0.983 (9)	0.983	0.984	0.983
0.35	0.850 (9)	0.850	0.851	—
0.40	0.746 (11)	0.746	0.747	0.746
0.45	0.665 (11)	0.664	0.664	—
0.50	0.609 (9)	0.609	0.597	—

Table 3. Comparison of the complex Kohn ^{3}S-wave phase shifts δ_0^- for e$^-$-Ps scattering with the prior Kohn [36] and 18-state close-coupling [38] results. Phase shifts are given in radians and ω is given by equation (21). For details on how we select a best ω see section 3.1 and appendix A.

k	Complex Kohn variational δ_0^- (best ω) [present]	Complex Kohn variational δ_0^- ($\omega = 8$) [present]	Kohn variational δ_0^- ($\omega = 9$) [36]	Close-coupling δ_0^- (18-state) [38]
0.05	−0.261 (13)	−0.262	−0.264	—
0.10	−0.536 (10)	−0.536	−0.537	−0.536
0.15	−0.797 (10)	−0.797	−0.799	—
0.20	−1.034 (10)	−1.034	−1.036	−1.033
0.25	−1.244 (10)	−1.245	−1.248	—
0.30	−1.430 (10)	−1.431	−1.434	−1.430
0.35	−1.593 (10)	−1.593	−1.598	—
0.40	−1.736 (11)	−1.738	−1.741	−1.736
0.45	−1.863 (8)	−1.863	−1.868	—
0.50	−1.974 (10)	−1.974	−1.979	—

Table 4. Resonance positions and widths of the e$^-$-Ps system. Positions are given in eV and widths are given in meV in curly brackets. The ω value that we use for each state is in parentheses and is given by equation (21).

State	Present (ω)	Ho/Bhatia & Ho/Kar & Ho [55, 72, 74, 75, 77]	Botero and Greene [86]	Gilmore *et al* [62]	Usukura and Suzuki [82]	Ward [36] Ward *et al* [37]	Igarashi *et al* [83]
^{1}S	4.734 (11)	4.734	4.7253/4.6815	4.739 43	4.733 972	4.768	4.733 40
	{1.17}	{1.2}	{—}	{1.204}	{1.153}	{1.6}	{1.17}
^{1}P	5.088 (11)	5.084 29	5.0998	5.094 450	—	5.094	5.084 31
	{0.0327}	{0.024}	{—}	{0.0693}	{—}	{—}	{0.03}
^{3}P(A)	4.808 (13)	4.807 53	—	4.811 719	—	4.808	4.807 52
	{3.48}	{3.467}	{—}	{3.548}	{—}	{3.50}	{3.54}
^{3}P(B)	5.095 (14)	5.085 89	—	5.098 854	—	5.101	5.086 08
	{0.81}	{0.446}	{—}	{0.484}	{—}	{1.00}	{0.44}
^{1}D(A)	4.955 (11)	4.954 849 32	—	4.961 945	—	—	4.954 89
	{0.04}	{0.050}	{—}	{0.0479}	{—}	{—}	{0.049}
^{1}D(B)	5.101 (13)	5.101 05	—	—	—	—	5.100 91
	{—}	{—}	{—}	{—}	{—}	{—}	{0.000 63}
^{3}D	5.097 (11)	5.099 7458	—	—	—	—	5.099 74
	{—}	{0.087}	{—}	{—}	{—}	{—}	{0.000 063}

Table 5. Comparison of the ^{1,3}S scattering lengths $a_0^{\pm}$ for e^--Ps scattering we calculate using the Kohn phase shifts with others given in the literature. The results in boldface are the ones we use in the evaluation of the zero-energy cross sections.

Calculation	a_0^+	a_0^-
Equation (26)	**11.9**	4.86
Equation (27)	11.9	**4.81**
Ward *et al* [37]	12.0	4.6
Bhatia and Drachman [66]	12.233	—
Kvitsinsky *et al* [89]	11.98	4.78
Ghoshal *et al* [90]	12.242	—

Table 6. Convergence of the binding energy E_b of the Ps^- ion with respect to variation of the ω value, where ω is given by equation (21).

ω	Number of terms (N)	Binding energy E_b
1	3	0.008 216 71
2	7	0.010 871 87
3	13	0.011 012 00
4	22	0.011 927 67
5	34	0.011 955 64
6	50	0.011 998 75
7	70	0.012 002 39
8	95	0.012 004 55
9	125	0.012 004 87
10	161	0.012 005 01

Table 7. The binding energy E_b of the Ps^- ion. (*(**) converted from Ryd (eV) to a.u.).

Calculation	Binding energy E_b
Present ($\omega = 10$)	0.012 005 01
Ward ($\omega = 8$) [36]	0.012 004 62
Ho* (946 terms) [53]	0.012 005 070 21
Kar and Ho [55]	0.012 005 0702
Frolov [58]	0.012 005 070 232 980 107 770 400 51
Korobov [59]	0.012 005 070 232 980 1077(3)
Drake *et al* [60]	0.012 005 070 232 980 107 627
Gilmore *et al*** [62]	0.0119

the binding energy of Ps^-. Table 6 shows the convergence of the calculation with respect to the ω value. In table 7 we compare our result with the previous variational result of Ward [36] and with the result of Ho who used a 946-term Hylleraas function [53]. We also compare our result with the result of Kar and Ho [55], of Frolov [58], and of Korobov [59] who used exponential functions. Additionally in this table we give the result of Drake *et al* who used a triple basis set in Hylleraas coordinates with 2528 terms [60] and with the result of Gilmore *et al* who used a 9-state coupled pseudostate approximation [62].

Our results that we give in table 7 are an improvement over prior results [36] using the same form of the ^{1}S bound-state trial wave function due to the higher ω value we use in the computation, which was made possible by converting the calculation (except for the eigenvalue matrix routune) from double to quadruple precision. The increased ω value allows for more terms in the trial wave function, and thus a theoretically more accurate wave function that produces a larger binding energy value. We optimize the two nonlinear parameters, α^+ and γ^+, in the ^{1}S bound-state trial wave function, equations (19) and (20), for our binding energy calculation and we give the values of these parameters in table A1 in appendix A. The Rayleigh–Ritz variational method provides a rigorous bound for the binding energy and thus the larger the value the more accurate the result. We think that the results of Frolov [58], Korobov [59], and Drake *et al*'s [60] are the most accurate ones in table 7. Our present result agrees well with their reported results, with a percent difference of approximately 0.0005% when compared to either of their results.

3.3. ^{1,3}P-wave phase shifts and resonances

We compute the ^{1,3}P-wave phase shifts and resonance parameters. As for the ^{1,3}S-wave, we compute the ^{1,3}P-wave phase shifts with the complex Kohn, Kohn, and inverse Kohn variational methods. We compare in tables 8 and 9 the complex Kohn ^{1,3}P-wave phase shifts with the prior results that used the Kohn variational method [37], and the 18-state close-coupling results of Igarashi *et al* [38]. There are instances where our complex Kohn results are slightly less than the prior Kohn-type variational results. However, it is deemed more beneficial to employ the complex Kohn method as it has fewer singularities than the other variational methods. The ^{1}P phase shifts are of importance due to their direct contribution to the Ps^- photodetachment cross section, and of particular interest in the ^{1}P-wave phase shifts is the cusp that appears to be due to the onset of the $Ps(n = 2)$ shape resonance. The effect of this cusp behavior can be seen in the photodetachment cross section results presented in the next section. We present in figure 2(a) closer view of the ^{1}P-wave cusp that we obtain with the complex Kohn method.

We discuss in appendix A numerical details for the ^{1,3}P scattering calculation and give the Kohn and inverse Kohn phase shift results in table A3. For a number of cases, we are able to obtain phase shifts with a higher ω value for the Kohn and inverse Kohn methods compared to prior calculations [37]. When compared to the previously reported Kohn ^{1,3}P phase shifts [37] our Kohn results generally agree to within two decimal places. However, for the ^{1}P phase shift for $k = 0.50$ the agreement is only to the first decimal place. The difference between our Kohn and inverse Kohn phase shift results is at least in the third decimal place.

In table 4, for the ^{1}P resonance and the ^{3}P resonance (A) we report values from the inverse Kohn method whereas for ^{3}P resonance (B) they are from the Kohn method. We compute the positions and widths for these resonances using the resonance fitting formula equation (24) over a range of ω values from 9–15. Of note is the width for the ^{1}P resonance we record in table 4, which had not been previously reported using a Kohn-type variational method.

Table 8. Comparison of the complex Kohn ^{1}P-wave phase shifts δ_1^+ for e$^-$-Ps scattering with the prior Kohn [37] and 18-state close-coupling [38] results. Phase shifts are given in radians and ω is given by equation (21). For details on how we select a best ω see section 3.1 and appendix A.

k	Complex Kohn variational δ_1^+ (best ω) [present]	Complex Kohn variational δ_1^+ ($\omega = 8$) [present]	Kohn variational δ_1^+ ($\omega = 9$) [37]	Close-coupling δ_1^+ (18-state) [38]
0.05	−0.0007 (8)	−0.0007	−0.0006	—
0.10	−0.038 (9)	−0.038	−0.038	−0.0379
0.15	−0.123 (9)	−0.123	−0.123	—
0.20	−0.235 (10)	−0.235	−0.235	−0.235
0.25	−0.353 (10)	−0.353	−0.353	—
0.30	−0.463 (11)	−0.463	−0.463	−0.463
0.35	−0.558 (11)	−0.559	−0.559	—
0.40	−0.635 (10)	−0.635	−0.635	−0.634
0.45	−0.687 (10)	−0.687	−0.687	—
0.50	−0.663 (8)	−0.663	−0.664	—

Table 9. Comparison of the complex Kohn ^{3}P-wave phase shifts δ_1^- for e$^-$-Ps scattering with the prior Kohn [37] and 18-state close-coupling [38] results. Phase shifts are given in radians and ω is given by equation (21). For details on how we select a best ω see section 3.1 and appendix A. Asterisks indicate a value that we believe to be a typo in the original publication.

k	Complex Kohn variational δ_1^- (best ω) [present]	Complex Kohn variational δ_1^- ($\omega = 8$) [present]	Kohn variational δ_1^- ($\omega = 9$) [37]	Close-coupling δ_1^- (18-state) [38]
0.05	0.031 (8)	0.031	0.031	—
0.10	0.192 (10)	0.192	0.192	0.192
0.15	0.483 (10)	0.483	0.484	—
0.20	0.706 (10)	0.706	0.707	0.707
0.25	0.784 (10)	0.784	0.784	—
0.30	0.778 (10)	0.777	0.778	0.778
0.35	0.737 (10)	0.737	0.737	—
0.40	0.687 (11)	0.686	0.687	0.687
0.45	0.641 (11)	0.640	0.641	—
0.50	0.661 (12)	0.660	***	—

3.4. *The photodetachment of Ps$^-$*

We present in figure 3 the photodetachment cross-section in the length, velocity, and acceleration forms that we compute using our bound-state wave function for $\omega = 10$, the corresponding binding energy, and the ^{1}P complex Kohn trial wave function with the best ω value. The cusp behavior in the ^{1}P-wave phase shifts just below the Ps($n = 2$) threshold is reflected in the photodetachment cross section. We compare our results with the length form of Igarashi *et al* [44] and Bhatia and Drachman [65] in which their length and velocity forms are identical. (We note that we use WebPlotDigitizer [109] to read the photodetachment cross section of Igarashi *et al* [44] given in figure 1 of their paper) We find that our length, velocity, and acceleration forms are in very good agreement with each other, and with the length form of Igarashi *et al* [44]. Also, our results using the complex Kohn ^{1}P continuum wave function agree very well with our results that we obtain (but we do not show in this paper), using the Kohn ^{1}P continuum wave function [110]. In appendix B we present numerical details of the calculation of the Ps$^-$ photodetachment cross section in the length, velocity, and acceleration forms.

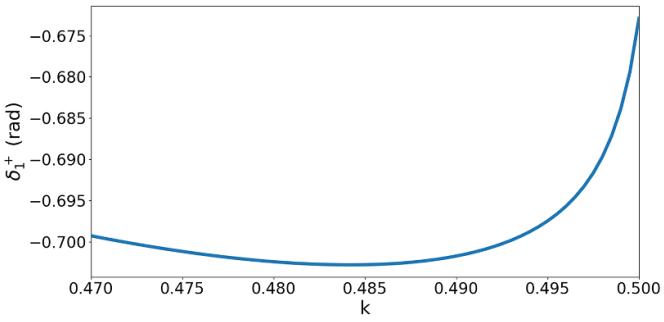

Figure 2. Cusp in the complex Kohn ^{1}P-wave phase shifts for e$^-$-Ps scattering.

3.5. *^{1,3}D-wave phase shifts and resonances*

Figures 4 and 5 show the ^{1}D- and ^{3}D-wave phase shifts, respectively, for the Kohn-type variational methods using the best ω values, and compares them to the 18-state close-coupling result [38]. There is excellent agreement between the results from the three Kohn-type variational methods we use,

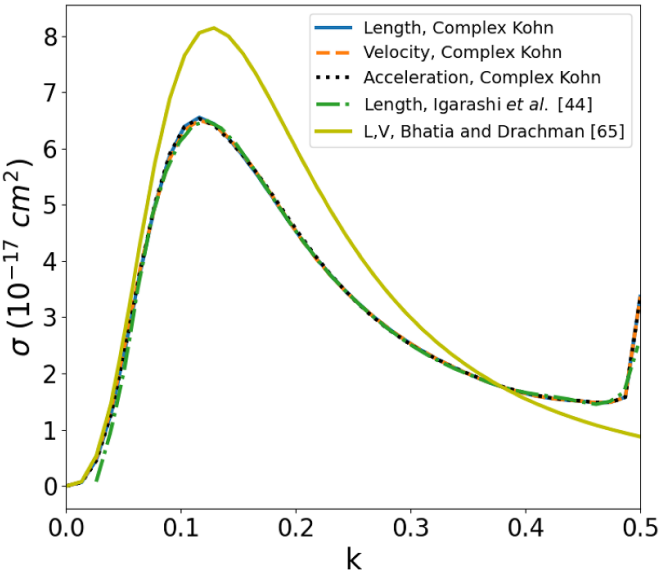

Figure 3. Comparison of the Ps^- photodetachment cross section in the length, velocity, and acceleration forms using the complex Kohn method for the ^{1}P continuum wave function, and with the photodetachment cross section in the length form using the close-coupling ^{1}P continuum wave function [44], and with the photodetachment cross section of Bhatia and Drachman [65].

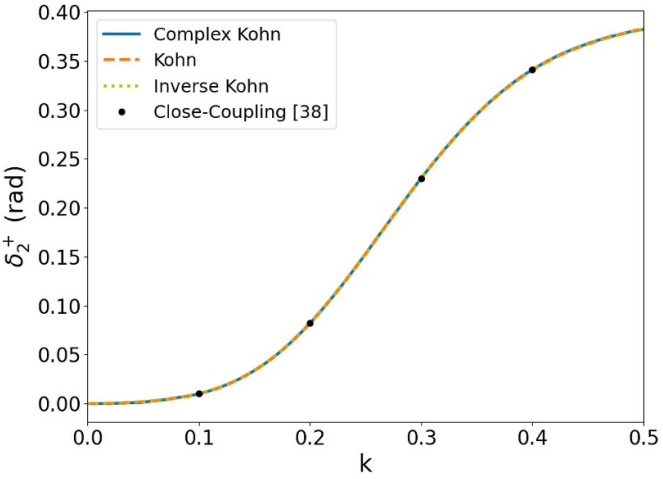

Figure 4. Comparison of the complex Kohn, Kohn, and inverse Kohn ^{1}D phase shifts for e^--Ps scattering together with the 18-state close-coupling [38] ^{1}D-wave phase shifts.

and also good agreement with the close-coupling results [38]. We optimize the nonlinear parameters for the ^{1,3}D-wave phase shifts and obtain results that are converged with respect to ω. Table 10 provides results for the Kohn and inverse Kohn ^{1,3}D phase shifts, while tables 11 and 12, respectively, compares the ^{1}D and ^{3}D complex Kohn phase shifts with the 18-state close-coupling results [38]. In appendix A we present further details of the phase shift calculations.

Table 4 shows the positions we obtain for three D resonances and the width for the first of the ^{1}D resonances. It also shows a comparison with results from the literature. We compute the parameters using the resonance fitting

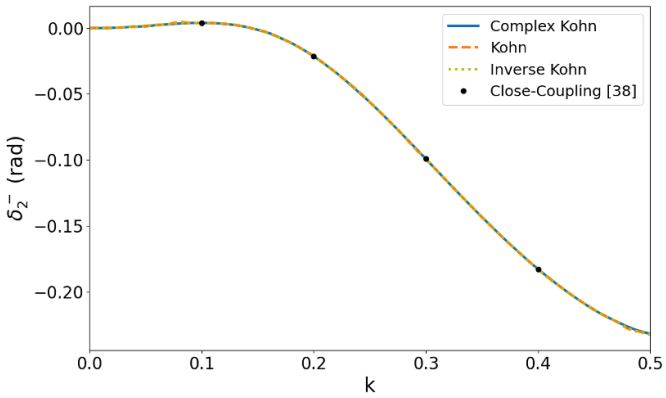

Figure 5. Comparison of the complex Kohn, Kohn, and inverse Kohn ^{3}D phase shifts for e^--Ps scattering together with the 18-state close-coupling [38] ^{3}D-wave phase shifts.

formula, equation (24), over a range of ω values from 8–13. The singlet resonance (A) parameters we report are from the complex Kohn method, the resonance (B) position is from the inverse Kohn method while the triplet resonance position is from the Kohn method. There is good agreement with the positions of the three resonances with those in the literature.

Of particular interest in the ^{1,3}D-wave calculation is the effect of the mixed-symmetry term in the trial wave function that is required for this higher partial wave. Tables 11 and 12 show a comparison of the results of the complex Kohn phase shifts we compute with and without the mixed symmetry term using our best ω values and a constant ω value of $\omega = 6$. When calculating the phase shifts with the constant ω value, we use the same nonlinear parameters for both the calculations with and without the mixed symmetry term for direct comparison. For the best ω case, it is clear that in general in the ^{1}D-wave case the mixed symmetry term contributes more substantially to the phase shift results as k increases. There is a single k-value ($k = 0.05$) that produces a higher phase shift in the calculation without the mixed symmetry term than with it when using the best ω value. This difference is minimal but can probably be attributed to the higher ω value that the calculation without the mixed symmetry term converges to. When comparing the calculations at the constant ω value, including the mixed symmetry term always produces a phase shift equal to or greater than the calculation without the mixed symmetry term, and again the increase in the phase shift result is more substantial for higher k values. For the ^{3}D-wave and best ω case, the mixed symmetry term contributes, in general, negligibly to the phase shifts. There are two values of k ($k = 0.05, 0.45$) where the phase shifts are slightly larger in the calculation without the mixed symmetry term than in the one with. However, for these two k-values, the best ω value is larger in the computation without the mixed symmetry term. For the other k-values, the phase shifts are identical to the precision given for the two computations. When comparing the ^{3}D phase shifts at the constant ω value of $\omega = 6$, the results with and without the mixed symmetry term are identical to the precision given.

Table 10. Kohn and inverse Kohn ^{1,3}D-wave phase shifts $\delta_2^{\pm}$ for e^--Ps scattering. Phase shifts are given in radians and ω is given by equation (21). For information on of how a best ω is chosen see text.

k	Kohn variational δ_2^+ (best ω)	Inverse Kohn variational δ_2^+ (best ω)	Kohn variational δ_2^- (best ω)	Inverse Kohn variational δ_2^- (best ω)
0.05	0.002 (11)	0.002 (9)	0.002 (10)	0.001 (12)
0.10	0.010 (9)	0.010 (11)	0.004 (9)	0.004 (9)
0.15	0.034 (9)	0.034 (11)	−0.001 (9)	−0.001 (9)
0.20	0.082 (10)	0.082 (8)	−0.021 (11)	−0.021 (10)
0.25	0.153 (10)	0.153 (8)	−0.056 (11)	−0.056 (10)
0.30	0.230 (11)	0.230 (11)	−0.099 (9)	−0.099 (10)
0.35	0.296 (11)	0.295 (11)	−0.144 (9)	−0.143 (10)
0.40	0.340 (9)	0.341 (10)	−0.183 (9)	−0.183 (9)
0.45	0.367 (9)	0.367 (10)	−0.214 (9)	−0.214 (9)
0.50	0.382 (9)	0.382 (11)	−0.233 (10)	−0.233 (9)

Table 11. Comparison of the complex Kohn ^{1}D-wave phase shifts δ_2^+ for e^--Ps scattering with and without the mixed symmetry term and with the prior 18-state close-coupling [38] results. Phase shifts are given in radians and ω is given by equation (21). For details on how we select a best ω see section 3.1 and appendix A.

k	Complex Kohn w/o mixed symmetry δ_2^+ (best ω)	Complex Kohn w/o mixed symmetry δ_2^+ ($\omega = 6$)	Complex Kohn with mixed symmetry δ_2^+ (best ω)	Complex Kohn with mixed symmetry δ_2^+ ($\omega = 6$)	Close-coupling δ_2^+ (18-state) [38]
0.05	0.002 (8)	0.001	0.001 (6)	0.001	—
0.10	0.010 (9)	0.010	0.010 (8)	0.010	0.0101
0.15	0.034 (9)	0.033	0.034 (8)	0.033	—
0.20	0.082 (8)	0.082	0.082 (7)	0.082	0.0823
0.25	0.153 (8)	0.151	0.153 (7)	0.153	—
0.30	0.227 (10)	0.227	0.230 (9)	0.230	0.230
0.35	0.291 (10)	0.290	0.295 (9)	0.295	—
0.40	0.333 (8)	0.332	0.341 (12)	0.340	0.341
0.45	0.356 (8)	0.353	0.368 (12)	0.365	—
0.50	0.364 (11)	0.363	0.382 (11)	0.381	—

Table 12. Comparison of the complex Kohn ^{3}D-wave phase shifts δ_2^- for e^--Ps scattering with and without the mixed symmetry term and with the prior 18-state close-coupling [38] results. Phase shifts are given in radians and ω is given by equation (21). For details on how we select a best ω see section 3.1 and appendix A.

k	Complex Kohn w/o mixed symmetry δ_2^- (best ω)	Complex Kohn w/o mixed symmetry δ_2^- ($\omega = 6$)	Complex Kohn with mixed symmetry δ_2^- (best ω)	Complex Kohn with mixed symmetry δ_2^- ($\omega = 6$)	Close-coupling δ_2^- (18-state) [38]
0.05	0.002 (8)	0.001	0.001 (6)	0.001	—
0.10	0.004 (8)	0.004	0.004 (7)	0.004	0.004 05
0.15	−0.001 (8)	−0.001	−0.001 (7)	−0.001	—
0.20	−0.021 (8)	−0.022	−0.021 (10)	−0.022	−0.0214
0.25	−0.056 (8)	−0.057	−0.056 (10)	−0.057	—
0.30	−0.099 (12)	−0.100	−0.099 (10)	−0.100	−0.0992
0.35	−0.143 (12)	−0.145	−0.143 (10)	−0.145	—
0.40	−0.183 (13)	−0.185	−0.183 (11)	−0.185	−0.183
0.45	−0.213 (13)	−0.220	−0.214 (11)	−0.220	—
0.50	−0.232 (11)	−0.233	−0.232 (8)	−0.233	—

We search for ^{1,3}D resonances in a calculation without the mixed symmetry term. We find a single ^{1}D resonance at 4.977 eV with a width of 0.004 meV. This corresponds to ^{1}D resonance A in table 4, however the parameters of the calculation using the mixed symmetry term agree better with the other results in the literature. Interestingly, in the calculation without the mixed symmetry term we do not obtain the singlet resonance B and the triplet resonance.

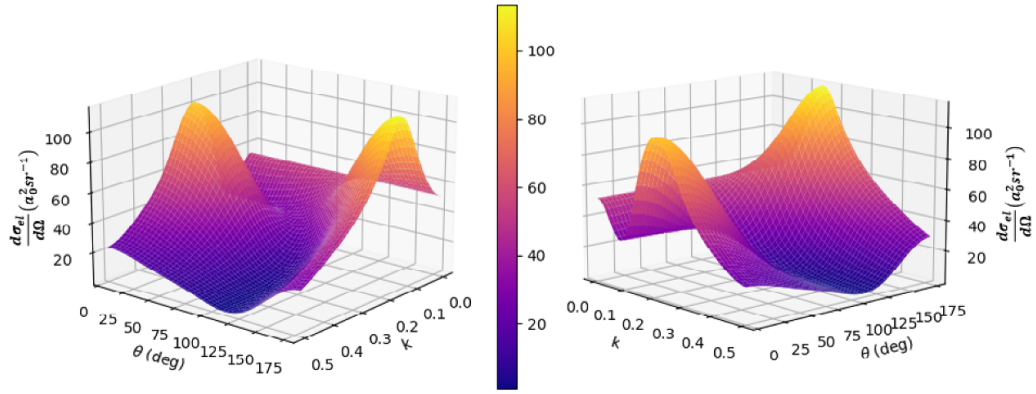

Figure 6. The spin-weighted elastic differential cross section for e^--Ps scattering at two viewing rotations.

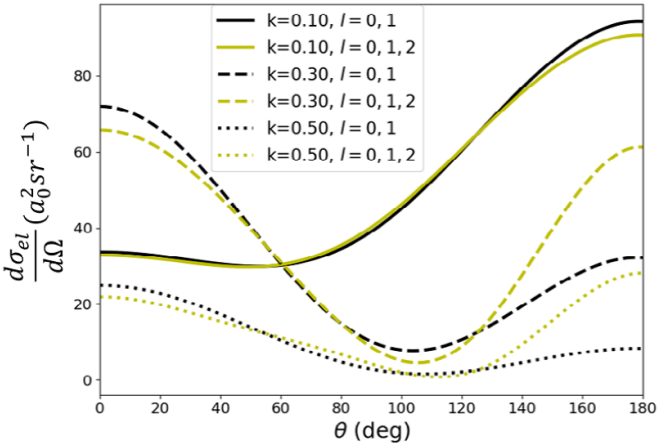

Figure 7. The spin-weighted elastic differential cross section for e^--Ps scattering versus the scattering angle θ for two different l ranges and at various k-values ($k = 0.1, 0.3,$ & 0.5).

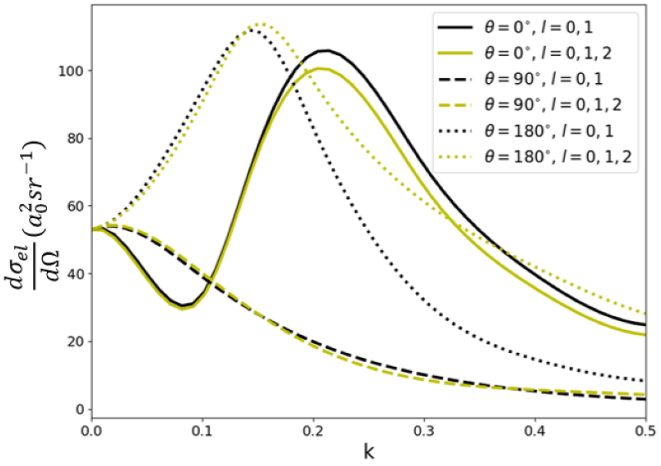

Figure 8. The spin-weighted elastic differential cross section for e^--Ps scattering versus k for two different l ranges and at various scattering angles ($\theta = 0°, 90°,$ & $180°$).

3.6. Scattering cross sections

In the calculation of the scattering cross sections, for the ^{1,3}S-, ^{1,3}P-, and ^{1,3}D-waves we use the complex Kohn phase shifts that we compute with the best ω values. For the ^{1,3}D-wave, we explicitly include the mixed symmetry term in the trial wave function.

We compute the spin-weighted elastic differential cross section using the ^{1,3}S-, ^{1,3}P-, and ^{1,3}D-wave complex Kohn phase shifts, and show the results in figures 6–8. Figure 6 shows 3D plots of the cross section. Figure 7 shows the cross section at various k-values versus the scattering angle and figure 8 shows the cross section at various scattering angles versus the k-value, both for two different l ranges. The complex Kohn ^{1,3}D-wave phase shifts have significant effect on the spin-weighted elastic differential cross section for the larger k values and near the forward and backward direction.

Figure 9 shows the results for the spin-weighted elastic integrated cross section for several different l ranges using the complex Kohn phase shifts for the ^{1,3}S-, ^{1,3}P-, ^{1,3}D-waves and the O'Malley *et al* ERT $l \geqslant 1$ formula [35] for the ^{1,3}F-wave. It can be seen that at higher k, the inclusion of the D-wave phase shifts leads to a noticeable change in the cross section result. However, when including the F-wave using the O'Malley *et al* [35] ERT $l \geqslant 1$ formula, the change in results is negligible. The elastic integrated cross section that we compute agrees well with the hyperspherical close-coupling calculation of Igarashi *et al* [91] and the 9-state coupled pseudostate calculation of Gilmore *et al* [62]. (The comparison is not shown). Using equation (48), we calculate a zero-energy elastic integrated cross section value of $211\pi a_0^2$. In comparison, Ward *et al* reported a zero-energy value of $208\pi a_0^2$ [37] and Kvitsinsky *et al* reported a value of $212.07\pi a_0^2$ [89], while Melezhik and Vukajlović gave a near-zero value of $292.1\pi a_0^2$ [92].

Figure 10 shows the results for the spin-weighted momentum-transfer cross section for a variety of l ranges using the complex Kohn phase shifts for the ^{1,3}S-, ^{1,3}P-, ^{1,3}D-waves and the O'Malley *at al.* ERT $l \geqslant 1$ formula [35] for the ^{1,3}F-wave. The inclusion of the D-wave phase shifts produces a noticeable increase to the cross section results at k-values above $k \approx 0.05$, which becomes more significant for larger k. Inclusion of the F-wave using the O'Malley *et al* [35] ERT $l \geqslant 1$ formula produces a minor change in the results above $k \approx 0.30$ but the results are almost identical below.

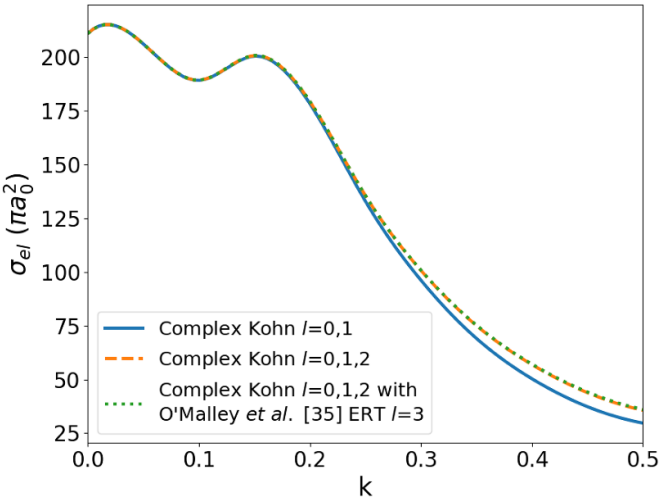

Figure 9. The spin-weighted elastic integrated cross section for e^--Ps scattering that we compute using the complex Kohn ^{1,3}S-,^{1,3}P-, and ^{1,3}D-wave phase shifts and the O'Malley *et al* ERT $l \geqslant 1$ formula [35] for the ^{1,3}F-wave phase shifts.

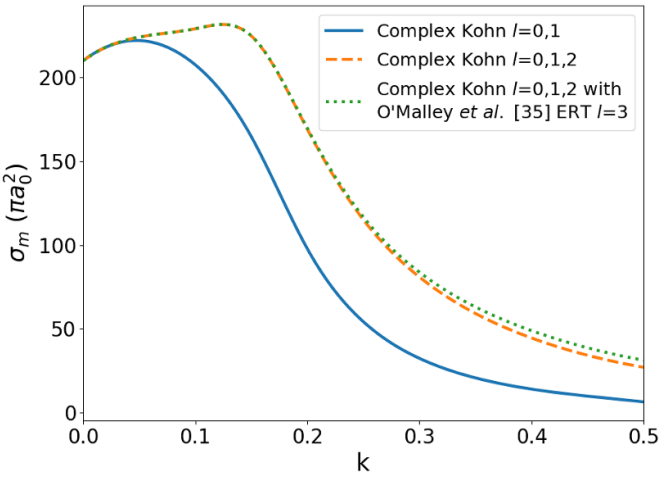

Figure 10. The spin-weighted momentum-transfer cross section that for e^--Ps scattering we compute using the complex Kohn ^{1,3}S-, ^{1,3}P-, and ^{1,3}D-wave phase shifts and the O'Malley *et al* ERT $l \geqslant 1$ formula [35] for the ^{1,3}F-wave phase shifts.

Figure 11 shows the results for the ortho-para conversion cross section for multiple l ranges that we compute using the complex Kohn for the ^{1,3}S-, ^{1,3}P-, and ^{1,3}D-waves and the O'Malley *et al* ERT $l \geqslant 1$ formula [35] for the ^{1,3}F-wave. The D-wave phase shifts produce an increase in the cross section above $k \approx 0.20$, which becomes more significant with increasing k. The effect on the cross section of the F-wave phase shifts that we compute using the O'Malley ERT $l \geqslant 1$ formula, equation (28) is negligible. The cross section agrees well with the hyperspherical close-coupling results of Igarashi *et al* [91] and with the 9-state coupled pseudostate results of Gilmore *et al* [62]. (The comparison is not shown). Using equation (50) we calculate a zero-energy ortho-para conversion cross section value of $12.6\pi a_0^2$, which agrees fairly well

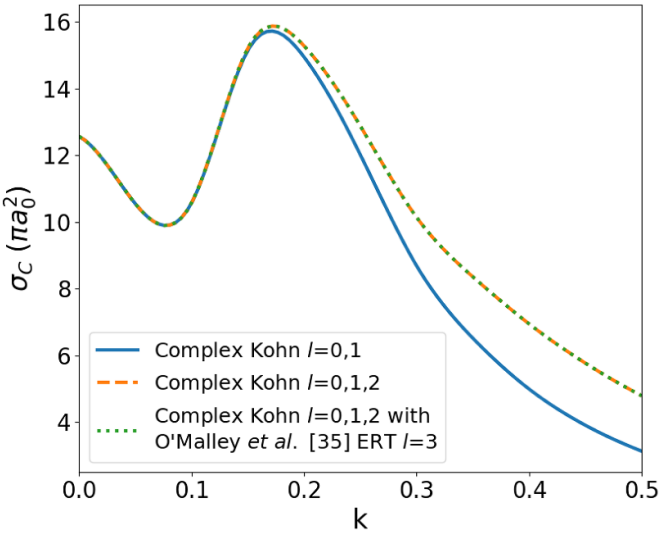

Figure 11. The ortho-para conversion cross section for e^--Ps scattering that we compute using the complex Kohn ^{1,3}S-, ^{1,3}P-, and ^{1,3}D-wave phase shifts and the O'Malley *et al* ERT $l \geqslant 1$ formula [35] for the ^{1,3}F-wave phase shifts.

with the prior results of Ward of $13.7\pi a_0^2$ [36] and well with the value reported by Kvitsinsky *et al* of $12.96\pi a_0^2$ [89].

4. Conclusion

We have examined the scattering of electrons by Ps below the Ps($n = 2$) threshold. Using the complex Kohn, Kohn, and inverse Kohn variational methods we have computed accurate ^{1,3}S-, ^{1,3}P-, and ^{1,3}D-wave phase shifts that may be considered benchmark. Our ^{1,3}S, ^{1,3}P and ^{1,3}D phase shifts agree well with the Kohn ^{1,3}S and ^{1,3}P phase shifts previously computed by Ward [36] and Ward *et al* [37] and with the 18-state close-coupling ^{1,3}S-, ^{1,3}P-, and ^{1,3}D-wave phase shifts computed by Igarashi *et al* [38]. We have investigated the effect that the mixed symmetry term in the complex Kohn ^{1,3}D-wave trial wave function has on both the phase shifts and resonances. The e^--Ps results can be used, with mass scaling, as benchmark results for proton-protonium calculations for antihydrogen investigations [42, 43].

We have examined closely the cusp behavior of the complex Kohn ^{1}P phase shifts just below the Ps($n = 2$) threshold, which reflects itself in the Ps^- photodetachment cross section. Using the ^{1}P continuum wave function for the e^--Ps system that we obtained from the complex Kohn variational method we computed the cross section in the length, velocity, and acceleration forms. This work was motivated by the experimental observation of the photodetachment of Ps^- [1, 21]. There is very good agreement between the different forms of the photodetachment cross section and our results agree very well with the length form of the cross section computed by Igarashi *et al* [44] who employed the hyperspherical close-coupling method for the ^{1}P continuum wave function.

We have calculated the elastic differential, elastic integrated, momentum-transfer, and ortho-para conversion cross

sections for e^--Ps scattering, and have shown the importance of the complex Kohn D-wave phase shifts in each of these cross sections. Using the S-wave scattering lengths that we determined from our Kohn S-wave phase shifts we have evaluated the zero-energy cross sections.

Data availability statement

The data that support the findings of this study are available upon reasonable request from the authors.

It is expected that the results will be available in William Mitchell's Ph.D. dissertation [110].

Acknowledgments

We wish to thank Drs. Klaus Bartschat, Mike Charlton, John Humberston, Yasayuki Nagashima, Martin Plummer, Peter Van Reeth, and Takuma Yamashita for their communications. S J W acknowledges support from NSF Grant PHY-2207886. We appreciate nodal hours from TACC Lonestar 6 and support from UNT Research Computing.

Appendix A. Numerics for the calculations of the binding energy, phase shifts, scattering lengths, and resonance parameters

We give in table A1 the optimized nonlinear parameters for the binding energy calculation, and the ^{1,3}S-, ^{1,3}P-, and ^{1,3}D-wave e^--Ps phase shift calculations. We optimized the nonlinear variational parameters by varying each parameter independently and selecting parameter values that produced the largest phase shift result. Each parameter was varied between 0 and 1 and we started with same choice of parameters used by Ward *et al* [36, 37, 45–48]. For the integrations that appear in the binding energy calculation, we use Gauss–Laguerre quadrature with $\omega+2$ integration points, where ω is defined according to equation (21). We solve the matrix equation using LAPACK routine DSYGV [111].

We use Gauss–Laguerre quadrature for the integrals in the calculations of the ^{1,3}S-, ^{1,3}P-, and ^{1,3}D-wave phase shifts. For the ^{1,3}S- and ^{1,3}P-wave matrix elements involving long-range terms we use 95 integration points, whereas for similar matrix elements for the ^{1,3}D-wave we use 350 integration points. The Gauss–Laguerre quadrature, with n' quadrature points, is exact (to within numerical accuracy) for polynomials of order $(2n'-1)$. We use for the integration of matrix elements involving short-range-short-range terms $\omega+2(l+1)$ integration points, where l refers to the partial wave. To solve the matrix equation (equation (13) and similar equations for the higher partial waves) we use LAPACK routine DGESV for the Kohn and inverse Kohn methods, whereas we use ZGESV for the complex Kohn method [111].

For each partial wave l we optimize the nonlinear parameters $\alpha^{\pm}$,$\gamma^{\pm}$,$\mu^{\pm}$, at four different k values, and we use these nonlinear parameters in four k ranges. We give in table A1 the k ranges and parameter values for the different partial waves. For the ^{1,3}S-wave the k values for the optimization are $k=0.02, 0.20, 0.40$, and 0.49, while for the ^{1,3}P-wave the k values are $k=0.02, 0.07, 0.40$, and 0.49, and for the ^{1,3}D-wave they are $k=0.02, 0.07, 0.30$, and 0.49. We take for the power n in the shielding function (equation (18)) the value of $2l+3$. We select the ω value, which we refer to as the best ω, for the Kohn and inverse Kohn methods in a similar way to how we select the best ω for the complex Kohn method and in which we discuss in section 3.1. However, for the ^{1,3}S- and ^{1,3}P-waves we consider the Kohn and inverse Kohn results together and we also consider the difference between the Kohn and inverse Kohn tangent of the phase shifts. We give Kohn and inverse Kohn phase shifts in table A2 for the ^{1,3}S-wave, table A3 for the ^{1,3}P-wave, and table 10 for the ^{1,3}D-wave.

Figures A1 and A2 present the tangent of the Kohn ^{1,3}S phase shifts we use to fit equations (26) and (27) for the scattering lengths, along with the tangent of the ^{1,3}S phase shifts we obtain from the fitted functions. We use an ω value of 10 for the ^{1}S phase shifts, an ω value of 15 for the ^{3}S phase shifts, and we use the nonlinear parameter values that we quote in table A1.

Table A1. Values of the nonlinear variational parameters that we use for the binding energy and e^--Ps phase shift calculations given as $\alpha|\gamma|\mu$. The Kohn and inverse Kohn calculations have the same parameters. We give the parameters we use in the complex Kohn calculations in parentheses. The * indicates the nonlinear parameters for the calculations done without the mixed symmetry term.

	k-range			
State	$0 \leqslant k < 0.10$	$0.10 \leqslant k < 0.30$	$0.30 \leqslant k < 0.48$	$0.48 \leqslant k \leqslant 0.50$
^{1}S	0.20 | 0.001 | 0.20 (0.20 | 0.025 | 0.125)	0.30 | 0.01 | 0.15 (0.30 | 0.01 | 0.15)	0.40 | 0.005 | 0.40 (0.40 | 0.007 | 0.40)	0.40 | 0.02 | 0.60 (0.375 | 0.001 | 0.50)
^{3}S	0.20 | 0.001 | 0.40 (0.175 | 0.001 | 0.10)	0.30 | 0.035 | 0.20 (0.30 | 0.001 | 0.15)	0.40 | 0.035 | 0.30 (0.40 | 0.013 | 0.175)	0.40 | 0.045 | 0.30 (0.40 | 0.025 | 0.30)
State	$0 \leqslant k < 0.05$	$0.05 \leqslant k < 0.10$	$0.10 \leqslant k < 0.48$	$0.48 \leqslant k \leqslant 0.50$
^{1}P	0.15 | 0.005 | 0.30 (0.125 | 0.0055 | 0.45)	0.15 | 0.03 | 0.225 (0.075 | 0.02 | 0.275)	0.30 | 0.06 | 0.225 (0.30 | 0.10 | 0.22)	0.36 | 0.06 | 0.34 (0.36 | 0.05 | 0.225)
^{3}P	0.15 | 0.006 | 0.25 (0.15 | 0.006 | 0.30)	0.15 | 0.039 | 0.225 (0.175 | 0.0405 | 0.225)	0.275 | 0.08 | 0.35 (0.275 | 0.075 | 0.38)	0.30 | 0.055 | 0.425 (0.30 | 0.065 | 0.44)
^{1}D	0.125 | 0.002 | 0.005 (0.075 | 0.0035 | 0.065)	0.20 | 0.001 | 0.125 (0.17 | 0.02 | 0.30)	0.20 | 0.08 | 0.275 (0.325 | 0.02 | 0.25)	0.40 | 0.065 | 0.30 (0.37 | 0.07 | 0.40)
^{1}D*	0.125 | 0.002 | 0.01 (0.075 | 0.005 | 0.50)	0.20 | 0.04 | 0.175 (0.125 | 0.02 | 0.225)	0.30 | 0.03 | 0.25 (0.35 | 0.06 | 0.225)	0.36 | 0.065 | 0.33 (0.36 | 0.06 | 0.38)
^{3}D	0.225 | 0.006 | 0.15 (0.10 | 0.0005 | 0.35)	0.15 | 0.035 | 0.175 (0.125 | 0.035 | 0.20)	0.275 | 0.085 | 0.40 (0.275 | 0.035 | 0.15)	0.30 | 0.01 | 0.65 (0.30 | 0.20 | 0.25)
^{3}D*	0.15 | 0.006 | 0.075 (0.125 | 0.001 | 0.20)	0.15 | 0.035 | 0.175 (0.075 | 0.045 | 0.175)	0.275 | 0.08 | 0.60 (0.275 | 0.03 | 0.20)	0.30 | 0.03 | 0.45 (0.30 | 0.15 | 0.25)
Binding Energy E_b: $\alpha^+ = 0.329$, $\gamma^+ = 0.0482$				

Table A2. ^{1,3}S-wave phase shifts $\delta_0^{\pm}$ for e^--Ps scattering. Phase shifts are given in radians and ω is given by equation (21). For information on of how we choose a best ω see section 3.1 and appendix A.

k	Kohn variational δ_0^+ (best ω)	Inverse Kohn variational δ_0^+ (best ω)	Kohn variational δ_0^- (best ω)	Inverse Kohn variational δ_0^- (best ω)
0.05	2.553 (9)	2.553 (9)	−0.261 (13)	−0.261 (13)
0.10	2.056 (12)	2.056 (12)	−0.536 (11)	−0.536 (11)
0.15	1.671 (12)	1.671 (12)	−0.797 (11)	−0.797 (11)
0.20	1.379 (13)	1.379 (13)	−1.034 (12)	−1.034 (12)
0.25	1.155 (13)	1.155 (13)	−1.244 (12)	−1.244 (12)
0.30	0.984 (9)	0.983 (9)	−1.430 (12)	−1.430 (12)
0.35	0.851 (9)	0.850 (9)	−1.593 (12)	−1.593 (12)
0.40	0.747 (11)	0.746 (11)	−1.737 (10)	−1.737 (10)
0.45	0.665 (9)	0.665 (9)	−1.863 (12)	−1.863 (12)
0.50	0.603 (10)	0.604 (10)	−1.974 (12)	−1.974 (12)

Table A3. ^{1,3}P-wave phase shifts $\delta_1^{\pm}$ for e$^-$-Ps scattering. Phase shifts are given in radians and ω is given by equation (21). For information on of how we choose a best ω see section 3.1 and appendix A.

k	Kohn variational δ_1^+ (best ω)	Inverse Kohn variational δ_1^+ (best ω)	Kohn variational δ_1^- (best ω)	Inverse Kohn variational δ_1^- (best ω)
0.05	−0.0006 (12)	−0.0006 (12)	0.031 (13)	0.031 (13)
0.10	−0.038 (13)	−0.038 (13)	0.192 (12)	0.192 (12)
0.15	−0.123 (13)	−0.123 (13)	0.484 (12)	0.484 (12)
0.20	−0.235 (10)	−0.235 (10)	0.707 (13)	0.707 (13)
0.25	−0.353 (10)	−0.353 (10)	0.784 (13)	0.784 (13)
0.30	−0.463 (11)	−0.463 (11)	0.778 (13)	0.778 (13)
0.35	−0.558 (11)	−0.558 (11)	0.737 (13)	0.737 (13)
0.40	−0.635 (8)	−0.635 (8)	0.687 (9)	0.687 (9)
0.45	−0.687 (8)	−0.687 (8)	0.641 (9)	0.641 (9)
0.50	−0.636 (13)	−0.637 (13)	0.656 (11)	0.653 (11)

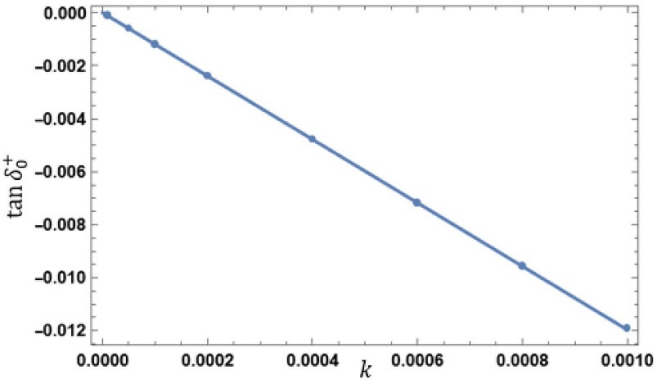

Figure A1. The tangent of the ^{1}S phase shift vs. k for e$^-$-Ps scattering. The dots represent the tangent of the Kohn ^{1}S phase shifts ($\omega = 10$) and the solid line is the $\tan\delta_0^+$ we obtain from fitting the Kohn ^{1}S phase shifts to equation (26). The R^2 value for this fit is 0.999 9996. Note equation (26) is for $k\cot\delta_0^+$ and the plot is for $\tan\delta_0^+$.

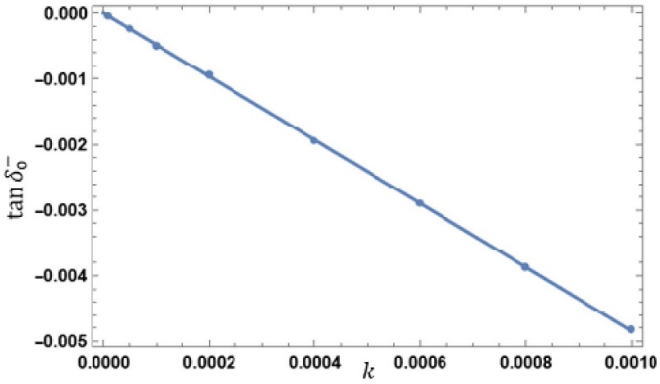

Figure A2. The tangent of the ^{3}S phase shift vs. k for e$^-$-Ps scattering. The dots represent the tangent of the Kohn ^{3}S phase shifts ($\omega = 15$) and the solid line is the $\tan\delta_0^-$ we obtain from fitting the Kohn ^{3}S phase shifts to equation (27). The R^2 value for this fit is 0.999 9748.

We obtain the resonance parameters using the Breit-Wigner formula with a slowly varying background (equation (24)). For our calculations we revise the Fortran code [101, 102] for equation (24). The revised code calls the subroutine DNLSFU from MATH77 [112] for the nonlinear least squares fit.

Appendix B. Numerics for calculations of the Ps$^-$ photodetachment cross section in the various forms

For the calculation of the Ps$^-$ photodetachment cross section in the length, velocity, and acceleration forms we use a highly correlated Hylleraas-type trial wave function that contains 161 terms for the ^{1}S bound-state, the corresponding binding energy E_b, the complex Kohn trial ^{1}P-wave function for the ^{1}P e$^-$-Ps continuum and the corresponding trial phase shifts. For the integrals for the short-range-short-range matrix elements in the calculation of the photodetachment cross section in all three forms we use $0.5(\omega_b + \omega_p) + 4$ quadrature points, where ω_b is the ω value for the binding energy calculation ($\omega_b = 10$) and ω_p is the best ω value for the complex Kohn ^{1}P e$^-$-Ps scattering calculation.

For the integrals for the matrix elements that involve long-range terms for the photodetachment cross section in the length and velocity forms, we use Gauss–Laguerre quadrature with 1300 quadrature points. However, due to the form of the dipole operator in the acceleration form (see equation (36)) of the photodetachment cross section, we treat the integrals for the matrix elements that involve long-range terms with special care near the origin. We split each integral over each respective interparticle distance into two integrals that range from 0 to a constant c, and from c to ∞. We perform the former using Gauss-Legendre quadrature and the latter using shifted Gauss–Laguerre quadrature [113],

$$\int_0^\infty f(x)\,dx = \int_0^c f(x)\,\mathrm{d}x + \int_c^\infty f(x)\,\mathrm{d}x. \qquad \text{(B.1)}$$

We set $c = 10^{-6}$ and we use 50 quadrature points in both the Gauss–Legendre and shifted Gauss–Laguerre quadrature.

ORCID iDs

William Mitchell https://orcid.org/0009-0004-6070-4031
S J Ward https://orcid.org/0000-0002-8496-360X

References

[1] Michishio K, Tachibana T, Terabe H, Igarashi A, Wada K, Kuga T, Yagishita A, Hyodo T and Nagashima Y 2011 *Phys. Rev. Lett.* **106** 153401
[2] Michishio K, Tachibana T, Suzuki R H, Wada K, Yagishita A, Hyodo T and Nagashima Y 2012 *Appl. Phys. Lett.* **100** 254102
[3] Michishio K, Chiari L, Tanaka F, Oshima N and Nagashima Y 2019 *Rev. Sci. Instrum.* **90** 023305
[4] Michishio K, Kanai T, Kuma S, Azuma T, Wada K, Mochizuki I, Hyodo T, Yagishita A and Nagashima Y 2016 *Nat. Commun.* **7** 11060
[5] Michishio K, Kuma S, Nagata Y, Chiari L, Iizuka T, Mikami R, Azuma T and Nagashima Y 2020 *Phys. Rev. Lett.* **125** 063001
[6] Michishio K, Chiari L, Tanaka F and Nagashima Y 2024 *Phys. Rev. Lett.* **132** 203001
[7] Nagashima Y 2014 *Phys. Rep.* **545** 95
[8] Nagashima Y, Michishio K, Chiari L and Nagata Y 2021 *J. Phys. B: At. Mol. Opt. Phys.* **54** 212001
[9] AEgIS experiment paves the way for new set of antimatter studies by laser-cooling positronium 2024 CERN (available at: https://home.cern/news/news/physics/aegis-experiment-paves-way-new-set-antimatter-studies-laser-cooling-positronium) (Accessed 11 October 2024)
[10] Glöggler L T *et al* 2024 *Phys. Rev. Lett.* **132** 083402
[11] Amsler C *et al* 2021 *Commun. Phys.* **4** 19
[12] Adrich P *et al* 2023 *Eur. Phys. J.* C **83** 1004
[13] Knutson E Laser-Cooling Positronium 2024 Physics Magazine (available at: https://physics.aps.org/articles/v17/s23) (Accessed 11 October 2024)
[14] Shu K, Miyamoto N, Motohashi Y, Uozumi R, Tajima Y and Yoshioka K 2024 *Phys. Rev.* A **109** 043520
[15] Shu K *et al* 2024 *Nature* **633** 793
[16] Schirber M Positronium Cooled to Record Low Temperature 2024 Physics Magazine (available at: https://physics.aps.org/articles/v17/145) (Accessed 11 October 2024)
[17] Cecchini G, Greaves R, Martinez D, Dailey K, Richardson L and Mills A Jr 2024 PPC13
[18] Mills A P Jr 2019 *AIP Conf. Proc.* **2182** 030001
[19] Emami-Razavi M and Darewych J W 2021 *Eur. Phys. J.* D **75** 188
[20] Adkins G S, Cassidy D B and Pérez-Ríos J 2022 *Phys. Rep.* **975** 1
[21] Nagashima Y 2018 Ps and Ps^- production using alkali-metal coated surfaces and its applications *18th Int. Conf. on Positron Annihilation Book of Abstracts* p 55
[22] Mitchell W J and Ward Quintanilla S J 2021 Singlet P-wave elastic electron-positronium scattering (available at: https://meetings.aps.org/Meeting/GEC21/Session/GT61.71)
[23] Ward Quintanilla S J and Mitchell W J 2022 ^{1,3}S and ^{1,3}P electron-positronium scattering (available at: https://meetings.aps.org/Meeting/DAMOP22/Session/F01.21)
[24] Mitchell W and Ward S J 2022 Electron-Ps elastic scattering and the photodetachment of Ps^- *19th Int. Conf. on Positron Annihilation ICPA-19 Book of Abstracts (PI38)* p 130 (available at: www.helsinki.fi/en/conferences/icpa-19/programme)
[25] Ward Quintanilla S J and Mitchell W J 2022 The Ps^- ion and e^--Ps scattering (available at: https://meetings.aps.org/Meeting/GEC22/Session/HT4.4)
[26] Ward Quintanilla S J and Mitchell W 2023 Photodetachment of the positronium negative ion (Ps^-) and the ^{1}D-wave e^--Ps scattering (available at: https://meetings.aps.org/Meeting/DAMOP23/Session/N01.22)
[27] Mitchell W and Ward S J 2023 Electron-positronium elastic scattering and the photodetachment of the positronium negative ion *POSMOL 2023 Book of Abstracts* p 97 (available at: https://sites.nd.edu/posmol2023conference/program/)
[28] Ward Quintanilla S J 2023 Electron-positronium scattering and the photodetachment of the positronium negative ion (available at: https://meetings.aps.org/Meeting/GEC23/Session/GT3.1)
[29] Ward Quintanilla S J and Mitchell W 2024 The photodetachment cross section of Ps^- and elastic e^--Ps scattering (available at: https://meetings.aps.org/Meeting/DAMOP24/Session/S00.17)
[30] Ward Quintanilla S J and Mitchell W 2024 Ps^- photodetachment and elastic electron-positronium scattering (available at: https://meetings.aps.org/Meeting/GEC24/Session/HT4.18)
[31] Quintanilla S J and Mitchell W 2025 One- and two-photon detachment of Ps^- and e^--Ps scattering cross sections *2025 DAMOP Meeting of the APS* (submitted)
[32] Tiesinga E, Mohr P J, Newell D B and Taylor B N 2021 CODATA recommended values of the fundamental physical constants: 2018 *J. Phys. Chem. Ref. Data* **50** 033105
[33] Cooper J N, Armour E A G and Plummer M 2009 *J. Phys. A: Math. Theor.* **42** 095207
[34] Cooper J N, Plummer M and Armour E A G 2010 *J. Phys. A: Math. Theor.* **43** 175302
[35] O'Malley T F, Spruch L and Rosenberg L 1961 *J. Math. Phys.* **2** 491
[36] Ward S J 1986 A theoretical study of elastic electron positronium scattering and photo-absorption by the positronium negative ion *PhD Thesis* Royal Holloway and Bedford New College, University of London (available at: https://repository.royalholloway.ac.uk) (Accessed 28 June 2024)
[37] Ward S J, Humberston J W and McDowell M R C 1987 *J. Phys. B: At. Mol. Phys.* **20** 127
[38] Igarashi A, Nakazaki S and Ohsaki A 2000 *Phys. Rev.* A **61** 032710
[39] Woods D, Ward S J and Van Reeth P 2015 *Phys. Rev.* A **92** 022713
[40] Wu M-S, Zhang J-Y, Gao X, Qian Y, Xie H-H, Varga K, Yan Z-C and Schwingenschlögl U 2020 *Phys. Rev.* A **101** 042705
[41] Wu M-S, Zhang J-Y, Qian Y, Varga K, Schwingenschlögl U and Yan Z-C 2021 *Phys. Rev.* A **103** 022817
[42] Plummer M 2024 private communication
[43] Kasoar E, Plummer M, Van Lydon L and Law M M 2023 *Front. Phys.* **11** 1187537
[44] Igarashi A, Shimamura I and Toshima N 2000 *New J. Phys.* **2** 17
[45] Ward S J, Humberston J W and McDowell M R C 1985 *J. Phys. B: At. Mol. Phys.* **18** L525
[46] Ward S J, Humberston J W and McDowell M R C 1986 *Proc. 3rd Int. Workshop on Positron (Electron)-Gas Scattering* ed W E Kaupilla, T S Stein and J M Wadehra (World Scientific Publishing Co Pte Ltd.) p 307
[47] Ward S J, McDowell M R C and Humberston J W 1986 *Europhys. Lett.* **1** 167
[48] Ward S J 2007 *NASA GSFC Science Symp. on Atomic and Molecular Physics (NASA/CP-2006-214146)* ed A K Bhatia (National Aeronautics and Space Administration, Goddard Space Flight Center) p 137

[49] McDowell M R C 1986 *Proc. 3rd Int. Workshop on Positron (Electron)-Gas Scattering* ed W E Kaupilla, T S Stein and J M Wadehra (World Scientific Publishing Co Pte Ltd.) p 11
[50] Basu A and Ghosh A S 2002 *Europhys. Lett.* **60** 46
[51] Ghosh A S and Basu A 2002 *Current Developments in Atomic, Molecular and Chemical Physics With Applications* (Springer) p 237
[52] Bhatia A K and Drachman R J 1983 *Phys. Rev.* A **28** 2523
[53] Ho Y K 1990 *Phys. Lett.* A **144** 237
[54] Ho Y K 1993 *Phys. Rev.* A **48** 4780
[55] Kar S and Ho Y K 2005 *Phys. Rev.* A **71** 052503
[56] Frolov A M 1999 *Phys. Rev.* A **60** 2834
[57] Frolov A M 2007 *J. Phys. A: Math. Theor.* **40** 6175
[58] Frolov A M 2015 *Chem. Phys. Lett.* **626** 49
[59] Korobov V I 2000 *Phys. Rev.* A **61** 064503
[60] Drake G W F, Cassar M M and Nistor R A 2002 *Phys. Rev.* A **65** 054501
[61] Haftel M I and Mandelzweig V B 1989 *Phys. Rev.* A **39** 2813
[62] Gilmore S, Blackwood J E and Walters H R J 2004 *Nucl. Instrum. Methods Phys. Res.* B **221** 124
[63] Blinov N and Czarnecki A 2012 *Phys. Rev.* A **85** 012522
[64] Bin D, Xiao-Yan G and Zhong-Qi M 2001 *Chin. Phys. Lett.* **18** 854
[65] Bhatia A K and Drachman R J 1985 *Phys. Rev.* A **32** 3745
[66] Bhatia A K and Drachman R J 1986 *Proc. 3rd Int. Workshop on Positron (Electron)-Gas Scattering* ed W E Kaupilla, T S Stein and J M Wadehra (World Scientific Publishing Co Pte Ltd.) p 310
[67] Ermolaev A M and Mandal C R 1988 *J. Phys. B: At. Mol. Phys.* **21** 2077
[68] Ghoshal A and Ho Y K 2010 *Few-Body Syst.* **47** 185
[69] Bhatia A K 2019 *Atoms* **7** 2
[70] Maniadaki K, Nikolopoulos L A A and Lambropoulos P 2002 *Eur. Phys. J.* D **20** 205
[71] Yamashita T 2023 private communication
[72] Ho Y K 1984 *Phys. Lett.* A **102** 348
[73] Bhatia A K and Ho Y K 1990 *Phys. Rev.* A **42** 1119
[74] Bhatia A K and Ho Y K 1993 *Phys. Rev.* A **48** 264
[75] Kar S and Ho Y K 2009 *Few-Body Syst.* **45** 43
[76] Kar S and Ho Y K 2010 *Eur. Phys. J.* D **57** 13
[77] Kar S and Ho Y K 2020 *Atoms* **8** 1
[78] Kar S and Ho Y K 2006 *Phys. Rev.* A **73** 032502
[79] Kar S, Wang Y and Ho Y K 2020 *Chin. J. Phys.* **68** 137
[80] Basu A and Ghosh A S 2008 *Nucl. Instrum. Methods Phys. Res.* B **266** 522
[81] Basu A 2011 *Eur. Phys. J.* D **65** 405
[82] Usukura J and Suzuki Y 2002 *Phys. Rev.* A **66** 010502(R)
[83] Igarashi A and Shimamura I 2004 *J. Phys. B: At. Mol. Opt. Phys.* **37** 4221
[84] Igarashi A 2016 *Eur. Phys. J.* D **70** 216
[85] Botero J 1987 *Phys. Rev.* A **35** 36
[86] Botero J and Greene C H 1985 *Phys. Rev.* A **32** 1249(R)
[87] Botero J and Greene C H 1986 *Phys. Rev. Lett.* **56** 1366
[88] Zhou Y and Lin C D 1995 *Phys. Rev. Lett.* **75** 2296
[89] Kvitsinsky A A, Carbonell J and Gignoux C 1992 *Phys. Rev.* A **46** 1310
[90] Ghoshal A, Kar S and Ho Y K 2010 *J. Phys.: Conf. Ser.* **199** 012015
[91] Igarashi A, Shimamura I and Toshima N 1998 *Phys. Rev.* A **58** 1166
[92] Melezhik V S and Vukajlović F R 1987 *Phys. Rev. Lett.* **59** 641
[93] Woods D 2015 Variational calculations of positronium scattering with hydrogen *PhD Dissertation* (University of North Texas) (available at: https://digital.library.unt.edu/ark:/67531/metadc822803/: Accessed 5 November 2024), University of North Texas Libraries, UNT Digital Library, (available at: https://digital.library.unt.edu) (arXiv:1508.05681)
[94] Van Reeth P G 1997 Theoretical studies of positronium formation in low energy positron-helium collisions *PhD Thesis* University College London, University of London (available at: https://discovery.ucl.ac.uk/id/eprint/10119561/) (Accessed 5 November 2024)
[95] Armour E A G and Humberston J W 1991 *Phys. Rep.* **204** 165
[96] Schwartz C 1961 *Phys. Rev.* **123** 1700
[97] Fano U and Rau A R P 1986 *Atomic Collisions and Spectra* (Academic)
[98] Breit G and Wigner E 1936 *Phys. Rev.* **49** 519
[99] Macek J 1970 *Phys. Rev.* A **2** 1101
[100] Hazi A U 1979 *Phys. Rev.* A **19** 920
[101] Morgan L A 1980s private communication
[102] Tennyson J and Noble C J 1984 *Comput. Phys. Commun.* **33** 421
[103] Bransden B H 1970 *Atomic Collision Theory, Lecture Notes and Supplements in Physics* (W.A. Benjamin, Inc.)
[104] Macek J H Effective range theory in atomic physics *Lectures Held During the Summer of 1980* (The Institute of Phyiscs, University of Aarhus) (unpublished)
[105] Levy B R and Keller J B 1963 *J. Math. Phys.* **4** 54
[106] Wolfram Research Inc. 2024 Mathematica, version 14.0 (available at: www.wolfram.com/mathematica) (Accessed 8 May 2024)
[107] Bransden B H and Joachain C J 2003 *Physics of Atoms and Molecules* 2nd edn (Prentice Education Limited)
[108] Baltenko A S and Segal I D 1983 *Zh. Tekh. Fiz.* **53** 796
Baltenko A S and Segal I D 1983 *Sov. Phys. - Tech. Phys.* **28** 508 (Engl. Transl.)
[109] Automeris-io WebPlotDigitizer (available at: https://apps.automeris.io/wpd4/) (Accessed 8 May 2024)
[110] Mitchell W Electron-positronium elastic scattering, one- and two-photon detachment of the positronium negative ion *PhD Dissertation* University of North Texas (in preparation)
[111] Netlib LAPACK (available at: https://netlib.org/lapack/explore-html-3.6.1/) (Accessed 3 June 2024)
[112] Index of /math/MATH77 2015 (available at: https://www.netlib.org/math/MATH77/) (Accessed 18 March 2025)
[113] Davis P J and Rabinowitz P 1984 *Methods of Numerical Integration* 2nd edn (Dover Publications, Inc.)